Technical Letter Memorandum RSI/TLM-186

To: Dr. Frank D. Hansen
Sandia National Laboratories
Mail Stop 0771
P.O. Box 5800
Albuquerque, NM 87185-0771

cc: Project Central File 2184 — Category C

From: Mr. Kirby D. Mellegard
Resident Consultant
RESPEC
P.O. Box 725
Rapid City, SD 57709

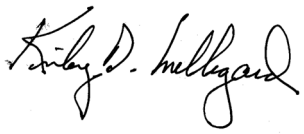

Date: September 4, 2013

Subject: Elevated Temperature Unconfined Compression Uniaxial Stress Tests on Salt Specimens From the Waste Isolation Pilot Plant

INTRODUCTION

This memorandum presents the results for the elevated temperature, unconfined, uniaxial stress tests performed on cylindrical specimens of Waste Isolation Pilot Plant (WIPP) salt under Sandia National Laboratories (SNL) Purchase Order No. 1307053.

The test results were based on scientific procedures for completing unconfined, uniaxial stress tests of intact salt at elevated temperature. Laboratory studies allow generic salt properties (mechanical, thermal, hydrological, and chemical) to be measured in a controlled environment. There is a large body of laboratory data that describes the phenomenology of salt across a broad range of temperatures expected in a heat-generating waste disposal system. Laboratory studies described in this document were designed to add substantively to that body of knowledge. Laboratory results generated in the tests described here will be used to develop input parameters for models, to assess the adequacy of existing models, and to predict material behavior. These laboratory studies are also consistent with the aims of international salt repository research programs.

The work was performed under the Quality Assurance guidelines provided for the Fuel Cycle Technology (FCT) Program. A test plan [Mellegard, 2013] was prepared in accordance with FCT QAP-20-1, because a test/activity plan was included as a deliverable (milestone) in the applicable work package. Deliverables described in the work package included the following:

1. Submit a test plan acceptable to FCT Quality Assurance Program Description. The test plan shall include load-path descriptions and recommendations
2. Complete prescribed test matrix

3. Summarize results in a technical letter memorandum.

The test plan was submitted and approved before testing began (Deliverable No. 1), the testing has been completed (Deliverable No. 2), and this technical letter memorandum is being submitted to satisfy Deliverable No. 3.

SCOPE

This testing program explored the phenomenology of intact salt at high temperatures. These laboratory-based experiments were designed to reduce uncertainties that remain in the technical bases for a generic safety case for disposing heat-generating waste in salt.

A conceptual test matrix comprising nine individual tests is presented in Table 1, and this matrix formed the basis of the test plan for this project. In 2012, RESPEC conducted scoping experiments at 200°C, 250°C, and 300°C [Mellegard, 2012]. On the basis of that exploratory work, various testing procedures were formalized including heating rate, thermal distribution, loading strategies, and the improvement of data acquisition, such as adding unload/reload cycles. Note that the maximum test temperature of 270°C was selected for the revised test matrix in Table 1, because the bedded salt samples decrepitated at 280°C during the scoping tests performed in 2012.

Table 1. Uniaxial Compression Test Matrix

Test Number	Salt Type	Test Type	Temperature	Loading Condition
1,2,3	Intact	Uniaxial stress	200°C	Unconfined Constant Strain Rate
4,5,6	Intact	Uniaxial stress	250°C	Unconfined Constant Strain Rate
7,8,9	Intact	Uniaxial stress	270°C	Unconfined Constant Strain Rate

Salt core was tested in an unconfined condition at a constant axial strain rate, by using solid cylinders. Uniaxial stress loading was continued until the specimen exhibited either failure or extreme deformation (> 20 percent strain). Inelastic creep processes were expected to dominate the deformation of the specimens, even in a quasi-static load application, with the creep response being ever-more pronounced as the temperature increases. Extreme deformation was expected to cause the tests to be terminated, rather than specimen failure.

SPECIMEN ACQUISITION AND PREPARATION

The salt core tested in this program were provided by SNL and were recovered from the WIPP site near Carlsbad, New Mexico. The core recovery locations are the horizontal boreholes

shown in the borehole location map in Figure 1, which was prepared for the Disturbed Rock Zone (DRZ) Characterization Test Plan at the WIPP. The sources of core are the three boreholes highlighted in yellow and are identified as QGU36, QGU37, and QGU38.

SNL performed a limited petrographic analysis on the salt core recovered from the boreholes. The analysis was completed by Dr. D. W. Powers, consulting geologist, and a summary of that work is attached to this memorandum. The result of primary interest for the current uniaxial testing is the conclusion that the core from the three boreholes identified as QGU36, QGU37, and QGU38 were considered to have few impurities, and the geology was similar among all three boreholes.

The core were recovered in 2001 and were placed in environmentally secure storage at the WIPP site. The core was shipped to RESPEC in Rapid City, South Dakota, by personal courier to ensure that the core was not subjected to any freight damage, temperature extremes, or mishandling. The shipping occurred in July 2012, and a record of the shipment is shown in Figure 2. The core is in secure storage at RESPEC and will be disposed of as SNL directs at the conclusion of the project.

An inventory of the core pieces shipped to RESPEC is listed in Figure 3. The 12 pieces that were transferred to RESPEC are highlighted in yellow. The individual core identification labels were later used when creating unique labels for individual test specimens that were fabricated from this core.

The chain-of-custody record for the core shipped to RESPEC is shown in Figures 4a and 4b. This record will be completed when the core is disposed of after the project is completed.

To prepare a testable specimen, a piece of salt core was sawn to an approximate length-to-diameter ratio (L:D) = 2. The walls and ends of the cylinder were then machined in a horizontal lathe to produce a finished right-circular cylinder whose ends were flat, parallel, and perpendicular to the specimen sides. A typical machining setup is shown in Figure 5, where the carbide tooling is visible next to the specimen surface. The finished specimens were then measured to determine their length and diameter. The specimens were also weighed, and a bulk density was calculated using the specimen dimensions to determine specimen volume. A summary of the testable specimens that were prepared is presented in Table 2. The bulk density values are very uniform and very near the typical value for halite (2.15 grams per cubic centimeter [g/cc]), which supports the previously referenced geological assessment that the specimens are relatively free of impurities.

All of the specimens in Table 1 have a unique identification number for tracking within the RESPEC laboratory. A typical specimen identification number is:

WIPP/QGU38-71/1

where:

WIPP = Waste Isolation Pilot Plant
QGU38 = borehole identifier
71 = core piece identifier
1 = specimen piece number.

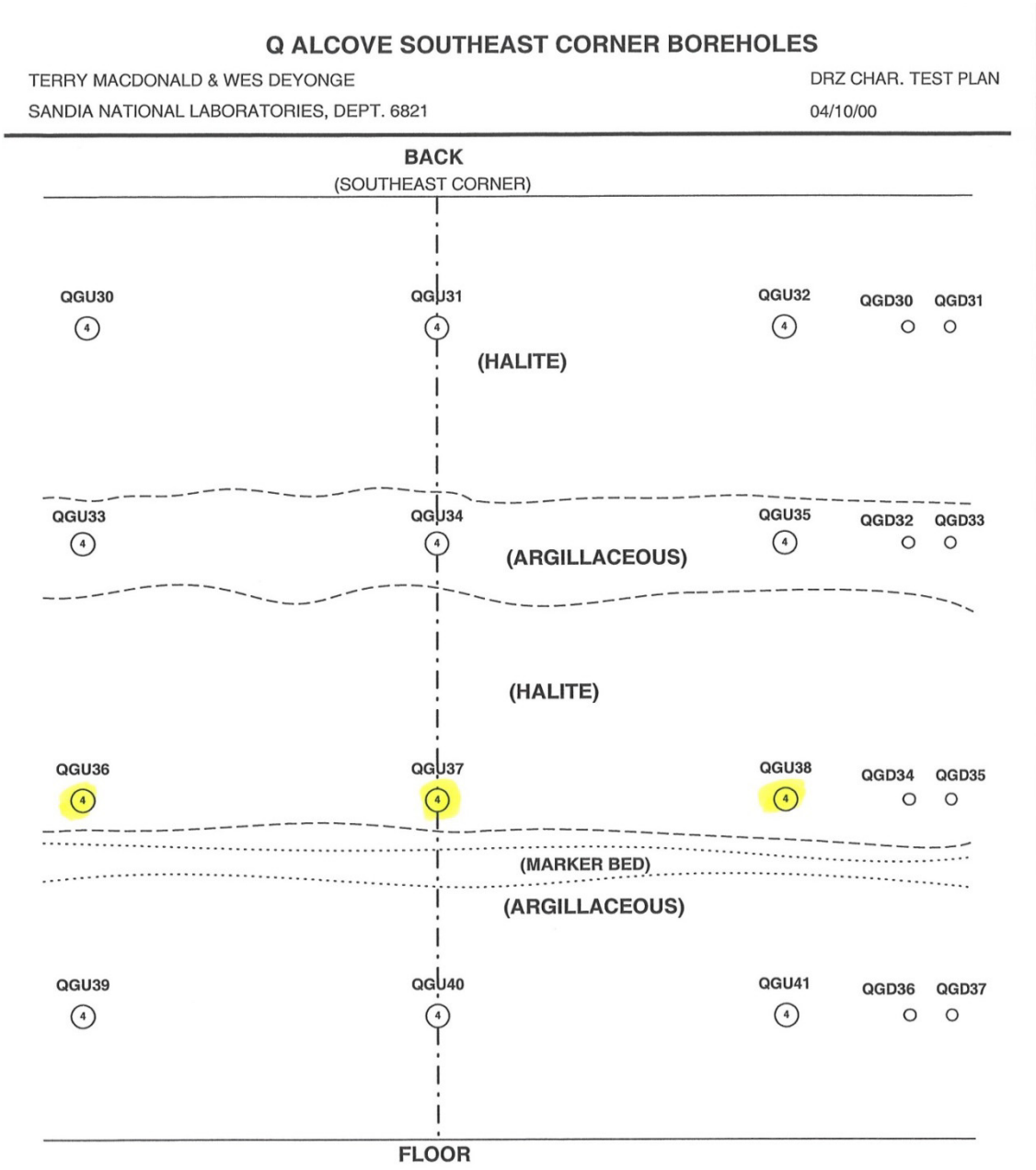

Figure 1. Core Recovery Borehole Locations at the Waste Isolation Pilot Plant.

Sandia National Laboratories
4100 National Parks Hwy.
Carlsbad NM 88221

SHIPPER **143980**
Commercial Invoice
Status: Waiting for Approval

Ship to:

RESPEC Engineering
3824 Jet Dr.

Rapid City SD 57703
USA

RMA# or RGA#	N/A
Deliver to:	Kirby Mellegard
Phone:	605-394-6507
Email:	N/A@SANDIA.GOV
Building: N/A	Room: N/A
Mail Stop:	N/A
Company:	RESPEC Engineering
Department:	N/A
Address Type:	Unclassified
Date Due at Destination:	07/26/2012
Production Related:	No

Origination Site:	Sandia New Mexico
Ship From Site:	Other
Form filled out by:	MACDONALD,TERRY L.
Phone:	505/845-0408
Date Prepared:	2012-07-16
Requester:	DEYONGE,WESLEY F
Phone:	505/284-5358
Org. #:	06212

For Shipment Processing Use

Date Shipped:	
Carrier:	None Selected
Mode:	None Selected
Bill of Lading No.:	
Total # of Pkgs:	0
Total Weight:	0.0 lbs
Total Cubic Dim:	0.0
Advance Notification	**Contacted** Yes No
Name and Phone:	
741 Number:	
ATS:	
TID Numbers:	
RCT Initial/Dates	

Arrived and unloaded at Rapid City, SD RESPEC office on 7/26/12. Inspected upon arrival - found 3 labeling errors on FCT forms SP forms were correct, RDA 7/26/12

Reason/Authority: To be Consumed in Testing / Incorporate into End Product
Return Date: NONE
Authority Number:
Freight Charge Payment: No Freight Charges
Project:
Task:
Carrier: None Selected
Mode: None Selected
Account:

If shipping controlled property to a new Sandia location
Destination Bldg: **Room:**

If shipping to international destination:
Foreign Customs import duties and fees will be paid by: N/A
Export Authorization:

No freight charge reason: Government Truck
Is material being shipped from the Shipping Department building or the 6000 Igloo? No
Shipment Comments: Handcarry.
Transportation Pickup Requested: No pickup requested
Questions about pickup call Dispatcher **844-1448** non-hazardous materials, **844-2556** hazardous materials.

Figure 2. Core Shipping Record for Waste Isolation Pilot Plant Salt.

RSI-2184-13-003

WIPP CORE WITH POTENTIAL FOR LABORATORY TESTS

LOCATED IN BLDG. NPHB, SHOP

June 18, 2012

Hole #	Box #	Section #	Length (ft.)	Length (in.)
QGU14	3	QGU14-21	1.35	~16
QGU14	4	QGU14-25	0.85	~10
QGU14	7	QGU14-45	1.27	~15
QGU14	8	QGU14-48	1.05	~12.5
QGU36	2	QGU36-2-1-2	0.9	~11
QGU36	2	QGU36-2-2	1.21	~14.5
QGU36	4	QGU36-11	1.37	~16
QGU36	5	QGU36-13-1	1.1	~13
QGU36	5	QGU36-13-2-2	0.85	~10
QGU36	6	QGU36-14	1.51	~18
QGU36	7	QGU36-17	1.32	~16
QGU36	7	QGU36-18	0.76	~9
QGU36	9	QGU36-27-2	0.8	~9.5
QGU36	9	QGU36-28	1.14	~13.5
QGU37	2	QGU37-15	0.99	~12
QGU37	3	QGU37-20	1.86	~22
QGU37	7	QGU37-45	1.01	~12
QGU37	8	QGU37-48	1.66	~20
QGU38	2	QGU38-6	1.07	~13
QGU38	2	QGU38-7	0.85	~10
QGU38	6	QGU38-43-1	1.09	~13
QGU38	6	QGU38-43-2	1.33	~16
QGU38	9	QGU38-70	0.97	~11.5
QGU38	9	QGU38-71	0.87	~10

Figure 3. Inventory of Core Pieces Shipped to RESPEC (Highlighted in Yellow).

RSI-2184-13-004

ACTIVITY/ PROJECT SPECIFIC Sandia PROCEDURE National Laboratories

Chain of Custody

Form Number: SP 13-1-1

Page 1 of 2

Attach more forms as needed

1. Initial Sample Custodian: Terry L. MacDonald (Printed Name) Organization: 6212 Date: 07/16/2012

2. Sample Collection or Creation Information

Test Plan ID: SNL-FCT-TP-11-0001 Scientific Notebook ID:

Field Log ID:

Sample Location: WIPP Underground, Q Room Southeast Corner, S-130/W-905 (i.e. borehole/core no./lab bldg. no./etc.)

Sample Team Members/Organization.

Terry L. MacDonald/SNL/6212

Wesley F. DeYonge/RESPEC/6212

enter n/a if none

3. Sample Identification Sample/Sub-Sample #	Date Collected	Container Type	Container Volume	Preservative	Analysis Request	Sample Description
QGU36-17	09-06-00	Poly Bag	0.11 cu ft	N/A	Heat Comp. Test	4 in. Dia. Halite/Polyhalite Core Sample. QGU36 subsample.
QGU36-18	09-06-00	Poly Bag	0.07 cu ft	N/A	Heat Comp. Test	4 in. Dia. Halite/Polyhalite Core Sample. QGU36 subsample.
QGU36-27-2	09-06-00	Poly Bag	0.07 cu ft	N/A	Heat Comp. Test	4 in. Dia. Halite/Polyhalite Core Sample. QGU36 subsample.
QGU36-28	09-06-00	Poly Bag	0.10 cu ft	N/A	Heat Comp. Test	4 in. Dia. Halite/Polyhalite Core Sample. QGU36 subsample.
QGU37-15	09-07-00	Poly Bag	0.09 cu ft	N/A	Heat Comp. Test	4 in. Dia. Halite/Polyhalite Core Sample. QGU37 subsample.
QGU37-20	09-08-00	Poly Bag	0.16 cu ft	N/A	Heat Comp. Test	4 in. Dia. Halite/Polyhalite Core Sample. QGU37 subsample.
QGU37-45	09-08-00	Poly Bag	0.09 cu ft	N/A	Heat Comp. Test	4 in. Dia. Halite/Polyhalite Core Sample. QGU37 subsample.
QGU37-48	09-08-00	Poly Bag	0.14 cu ft	N/A	Heat Comp. Test	4 in. Dia. Halite/Polyhalite Core Sample. QGU37 subsample.

enter n/a if none

4. Sample Requirements

Handling: Use Bubble Wrap and Core Boxes.

Storage & Preservation: Packed in Poly Bag to Preserve Moisture Content; Store in a Temperature Controlled Environment.

Shipping: Wood Crate and/or PVC Pipe.

Archive: N/A

Disposition: Observation and Destructive Testing; Dispose of in Regular Trash After Testing.

Expiration Date: N/A

5. Custody Transfer	Printed Name	Signature	Organization/Company	Date-Time	Sample Condition
a. Relinquished by:	Terry L. MacDonald		SNL/6212	07-20-12/0800	Intact
a. Received by:	Wesley F. DeYonge		RESPEC/6212	07-20-12/0800	Intact
b. Relinquished by:	Wesley F. DeYonge		RESPEC/6212	7/26/12/1605	Intact
b. Received by:	Rodger Arnold		RESPEC	7/26/12/1609	Intact
c. Relinquished by:					
c. Received by:					

Upon sample receipt, note condition. This form (copy for your records) shall follow samples through its life, until final disposition, then send original to WIPP Records Center.
For samples that are potentially hazardous & require packaging and shipping, contact Center 6200 ES&H Coordinator or see SNL ES&H Manual, Chpt. 12.

Figure 4a. Chain-of-Custody Documentation for Waste Isolation Pilot Plant Salt Core (Page 1 of 2).

RSI-2184-13-004

ACTIVITY/ PROJECT SPECIFIC PROCEDURE
Sandia National Laboratories

Chain of Custody

Form Number: SP 13-1-1
Page 2 of 2
Attach more forms as needed

1. Initial Sample Custodian: Terry L. MacDonald (Printed Name) Organization: 6212 Date: 07/16/2012

2. Sample Collection or Creation Information
Test Plan ID: SNL-FCT-TP-11-0001 Scientific Notebook ID:
Sample Location: WIPP Underground, Q Room Southeast Corner, S-130/W-905 (i.e. borehole/core no./lab bldg. no./etc.) Field Log ID:
Sample Team Members/Organization.
Terry L. MacDonald/SNL/6212
Wesley F. DeYonge/RESPEC/6212
enter n/a if none

3. Sample Identification Sample/Sub-Sample #	Date Collected	Container Type	Container Volume	Preservative	Analysis Request	Sample Description
QGU38-43-1	09-12-00	Poly Bag	0.09 cu ft	N/A	Heat Comp. Test	4 in. Dia. Halite/Polyhalite Core Sample. QGU38 subsample.
QGU38-43-2	09-12-00	Poly Bag	0.12 cu ft	N/A	Heat Comp. Test	4 in. Dia. Halite/Polyhalite Core Sample. QGU38 subsample.
QGU38-70	09-12-00	Poly Bag	0.08 cu ft	N/A	Heat Comp. Test	4 in. Dia. Halite/Polyhalite Core Sample. QGU38 subsample.
QGU38-71	09-12-00	Poly Bag	0.08 cu ft	N/A	Heat Comp. Test	4 in. Dia. Halite/Polyhalite Core Sample. QGU38 subsample.
----------Last Item----------						

enter n/a if none

4. Sample Requirements
Handling: Use Bubble Wrap and Core Boxes.
Storage & Preservation: Packed in Poly Bag to Preserve Moisture Content; Store in a Temperature Controlled Environment.
Shipping: Wood Crate and/or PVC Pipe.
Archive: N/A
Disposition: Observation and Destructive Testing; Dispose of in Regular Trash After Testing.
Expiration Date: N/A

5. Custody Transfer	Printed Name	Signature	Organization/Company	Date-Time	Sample Condition
a. Relinquished by:	Terry L. MacDonald		SNL/6212	07-20-12/0800	Intact
a. Received by:	Wesley F. DeYonge		RESPEC/6212	07-20-12/0800	Intact
b. Relinquished by:	Wesley F. DeYonge		RESPEC/6212	7/26/12/1605	Intact
b. Received by:	Rodger Arnold		RESPEC	7/26/12 1609	Intact
c. Relinquished by:					
c. Received by:					

Upon sample receipt, note condition. This form (copy for your records) shall follow samples through its life, until final disposition, then send original to WIPP Records Center.
For samples that are potentially hazardous & require packaging and shipping, contact Center 6200 ES&H Coordinator or see SNL ES&H Manual, Chpt. 12.

Figure 4b. Chain-of-Custody Documentation for Waste Isolation Pilot Plant Salt Core (Page 2 of 2).

RSI-2184-13-005

Figure 5. Typical Horizontal Lathe Machining Setup for Preparing Cylindrical Specimens.

Table 2. Summary of Salt Specimens Prepared for Testing

Specimen I.D.	Length (mm)	Diameter (mm)	Mass (g)	Density (g/cc)
WIPP/QGU37-20/1	204.13	90.97	2,859.60	2.16
WIPP/QGU37-20/2	207.32	90.96	2,908.50	2.16
WIPP/QGU37-15/1	205.34	89.74	2,809.40	2.16
WIPP/QGU37-45/1	206.59	91.03	2,903.70	2.16
WIPP/QGU36-17/1	204.04	89.53	2,776.60	2.16
WIPP/QGU36-18/1	204.87	89.59	2,786.35	2.16
WIPP/QGU36-27-2/1	206.76	89.39	2,791.95	2.15
WIPP/QGU36-28/1	206.12	89.51	2,792.55	2.15
WIPP/QGU37-48/1	206.54	89.53	2,798.40	2.15
WIPP/QGU37-48/2	207.88	89.56	2,820.40	2.15
WIPP/QGU38-43/1	206.98	89.59	2,816.85	2.16
WIPP/QGU38-43-2/1	207.71	89.43	2,820.55	2.16
WIPP/QGU38-71/1	207.23	89.54	2,820.80	2.16

During the machining process where the core was finished in a horizontal lathe, the operator observed that the cutting tool frequently encountered pockets of moisture (presumably brine) as the walls of the specimen were being trimmed to final dimension. Even though the core appeared to be dry on the surface when it was initially mounted in the lathe, wet spots began to appear as the cutting tool proceeded to make repeated small machining passes (reducing the radius by only approximately 0.3 mm per pass); wet spots are evidence of noninterconnected brine inclusions. The number of inclusions increased as the cutting depth increased with each machining pass, but they were observed even during the first pass. This indicates that some isolated brine inclusions existed within approximately 0.3 mm of the specimen surface. A photograph of a newly machined specimen is shown in Figure 6 and the wet brine spots are visible as dark round circles scattered on the surface of the specimen.

TEST EQUIPMENT

The testing was completed using a universal test system with four reaction columns referred to as the UTS4 system. The UTS4 is a computer-controlled, servohydraulic system manufactured by MTS Systems of Eden Prairie, Minnesota. The computer control allows for controlling the loading in either of two modes, a stress rate mode using the load cell output as a feedback signal or strain rate mode that uses a linear variable differential transformer (LVDT) output to control loading. An environmental chamber is mounted in the test system to provide the high-temperature environment required to perform unconfined tests at temperatures up to 300°C.

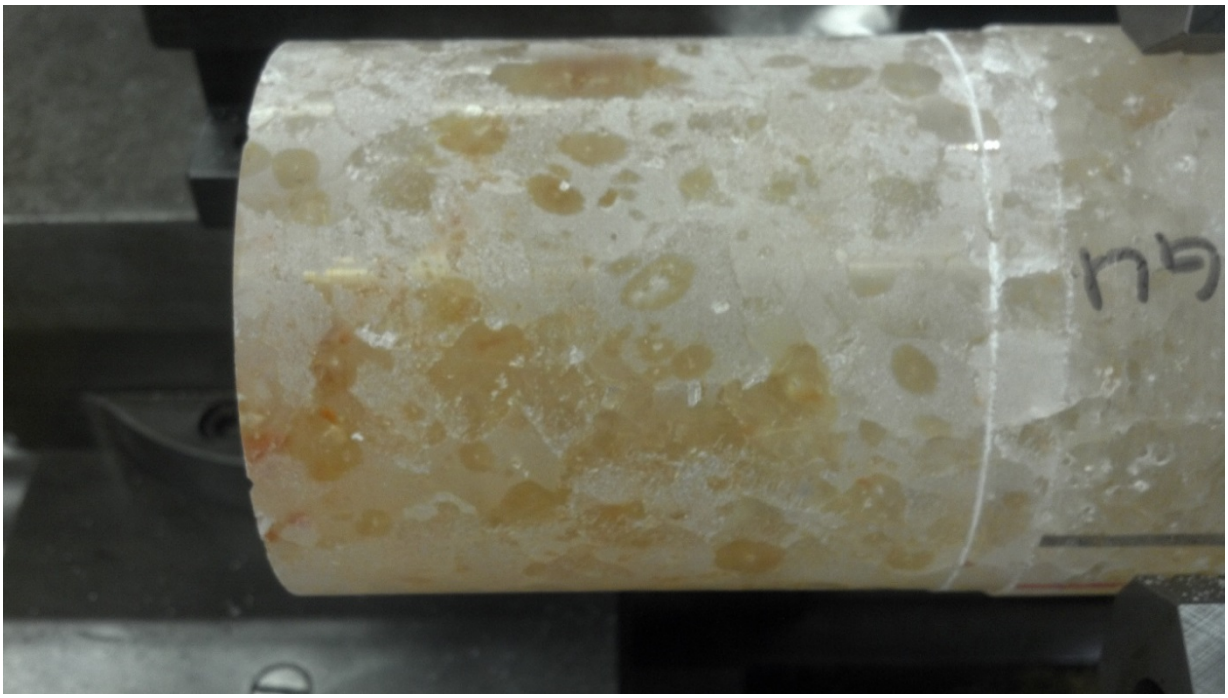

Figure 6. Waste Isolation Pilot Plant Salt Specimen Brine Inclusions (Darker Ovoid Areas Are Wet).

A photograph of the test system is provided in Figure 7 and illustrates the environmental chamber mounted in the test frame with the chamber door open for easy viewing of the interior of the chamber. Two salt specimens are inside the chamber. The specimen on the left is an Avery Island dome salt specimen instrumented with thermocouples to monitor salt specimen temperatures. There are some other thermocouples suspended in air that monitor the temperature of the air inside the chamber. Located in the load train in the middle of the chamber is a tested salt specimen (somewhat barrel shaped). Above and below the specimen are steel loading platens attached to long insulating rods that provide insulation between the hot specimen inside the chamber and the loading actuators outside the chamber. Just in view at the top of the photograph is the load cell that monitors axial loading force. A LVDT that monitors axial displacement is mounted inside the hydraulic actuator at the base of the system (not in view).

All three sets of instrumentation including the load cell, the LVDT, and the thermocouples were calibrated against in-house standards that are certified as traceable to National Institute of Standards and Technology (NIST) references. Calibration records indicate that the load cell force readings and the LVDT displacement measurements are accurate to within ± 1 percent of reading, and the thermocouple temperatures are accurate to within ± 2°C. Because the LVDT measures total axial displacement including some nonspecimen contributions, a “machine softness” factor that allowed correction of the LVDT measurements was determined. Using a steel specimen for which accurate elastic parameters are known, the “machine softness” correction coefficient was determined to be 0.004 millimeter per kilonewton (mm/kN). This

coefficient can be multiplied by the load cell reading and the product subtracted from the accompanying LVDT measurement to estimate the displacement of the specimen at that point.

RSI-2184-13-008

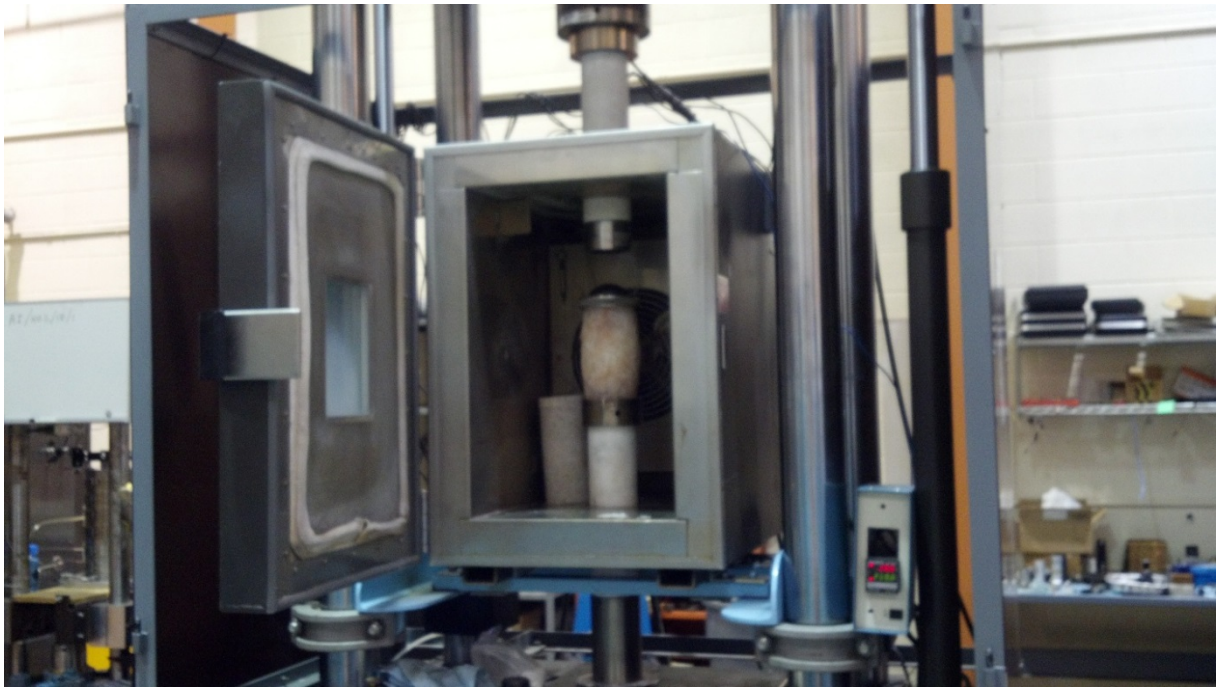

Figure 7. Uniaxial Test System Equipped With High-Temperature Environmental Chamber.

TEST PROCEDURE

The test procedure was based on original investigations performed in a previous RESPEC study and reported in a previous technical letter memorandum [Mellegard, 2012]. The general procedure is repeated here for convenience.

The planned test procedure comprises the following steps:

1. Bring the specimen to temperature at a rate of 1°C/minute. Thermal stabilization at the target test temperature would occur overnight. Multiple thermocouples were used to verify that the air in the environmental chamber was well mixed by the chamber fan to eliminate thermal gradients surrounding the specimen.
2. Apply a small preload to the specimen (approximately 0.2 MPa) to establish a reliable position to zero the LVDT (mounted in the hydraulic cylinder) used to measure axial displacement. The preload was based on a load measurement provided by a load cell located outside the environmental chamber.
3. Using the LVDT output, calculate axial strain in real time and apply deformation (load) at a strain rate of 10^{-4} s^{-1} until reaching an axial strain level of 5 percent. This portion of the load-path required 500 seconds (< 10 minutes).

4. Perform an unload/reload cycle. This step provides data for estimating a value for Young's modulus. The unload/reload cycle is performed in load control and is completed quickly, so the measured strain will be dominated by elastic deformation. At the end of the reload, resume loading at the original strain rate of 10^{-4} s^{-1} until reaching a strain level of 10 percent. This entire step will require approximately another 10 minutes.

5. Perform another unload/reload cycle at the 10 percent strain level to obtain data for another estimate of Young's modulus. When the reloading is completed, resume loading at the original strain rate of 10^{-4} s^{-1} until reaching a strain level of 12 percent. This entire step will require less than 5 minutes.

6. At a strain level of 12 percent, reduce the controlled strain rate from 10^{-4} s^{-1} to zero. This initiates a stress-relaxation test that will provide data for assessing the time-dependent deformation of the salt. The stress should display an exponential decay, and it is assumed that the stress will be asymptotically approaching zero within a few hours. Nonetheless, the stress-relaxation phase will be allowed to continue overnight, so the next (and final) loading step will be initiated the following day.

7. The controlled strain rate is increased from zero to 10^{-4} s^{-1}, and loading continues until one of the following test termination criteria are met: (1) the specimen fails, (2) the specimen exhibits a flat stress-strain response (perfectly plastic), or (3) the specimen becomes malformed to an extent that cylindrical geometry assumptions become grossly inadequate. It is anticipated that criterion (3) could become evident at axial strains above 20 percent.

8. Test termination simply entails removing all load and heating. When the specimen has cooled, it is preserved for possible posttest analyses that are undetermined at this point.

TEST RESULTS

For ease of comparison, all of the data from the previous investigations [Mellegard, 2012] have been included in this section. The previous investigations were also published and presented at the American Rock Mechanics Association (ARMA) symposium held in San Francisco, California [Mellegard et al., 2013], and a copy of that publication is attached to this memorandum. All core samples were consumed in the test attempts. Not all of the tests were successful in that some of the specimens exhibited violent decrepitation at the highest temperatures before mechanical loading could begin and in one test the temperature control system failed. The status of each specimen used in the testing is summarized in Table 3.

Four of the tests exhibited violent decrepitation before any loading could be applied. The two tests with a target temperature of 300°C failed as the specimen temperature (estimated by thermocouples located along the central axis of the Avery Island salt specimen collocated in the test chamber) reached approximately 280°C. The other two tests reached their target temperature of 270°C but failed shortly thereafter before any loading was applied.

The decrepitation apparently did not depend on the rate of heating. For example, specimen WIPP/QGU37-20/2 was placed in the environmental chamber and the chamber temperature was ramped to 300°C at a rate of 1°C/minute. The decrepitation occurred at approximately

280°C with a violent explosion that reduced the specimen to rubble. Anticipating that the heating rate might have been too fast, the next specimen, WIPP/QGU37-45/1, was heated to just 250°C at a rate of 1°C/minute and then allowed to remain at 250°C for 24 hours. After 24 hours, the test chamber temperature was ramped to 300°C at a rate of 1°C/minute, and when the specimen temperature reached 285°C (as indicated by the thermocouples in the Avery Island specimen), violent decrepitation caused the top third of the specimen to explode into rubble. At that point, the heat was turned off, but approximately 5 minutes later the remaining two-thirds of the specimen also exploded, which effectively reduced the entire specimen to rubble.

Table 3. Test Matrix Summary

Specimen I.D.	Temperature Target (°C)	Status/Comment
WIPP/QGU38-43-2/1	175	Successful
WIPP/QGU37-20/1	200	Successful
WIPP/QGU37-48/1	200	Successful
WIPP/QGU38-43/1	200	Successful
WIPP/QGU37-15/1	250	Successful
WIPP/QGU36-28/1	250	Successful
WIPP/QGU38-71/1	250	Successful
WIPP/QGU36-17/1	250	Heater system failed
WIPP/QGU36-27-2/1	270	Successful
WIPP/QGU36-18/1	270	Violent decrepitation at approximately 270°C (no data)
WIPP/QGU36-48/2	270	Violent decrepitation at approximately 270°C (no data)
WIPP/QGU37-20/2	300	Violent decrepitation at approximately 275°C (no data)
WIPP/QGU37-45/1	300	Violent decrepitation at approximately 285°C (no data)

A posttest photograph shown in Figure 8 is typical of the rubble that remains after the violent decrepitation occurs. Note in Figure 8 that the Avery Island domal salt specimen still remained intact throughout both attempts at 300°C tests on the WIPP salt; this indicates that there is obviously a significant difference between the two salt types, which is attributed to the presence of the brine inclusions noted during specimen preparation.

The violent decrepitation observed in the tests is neither unique to WIPP salt, nor unexpected. Similar observations were made during the Project Salt Vault investigation in Lyons, Kansas, [Bradshaw and McClain, 1971]. They reported observations characterized as “trapped moisture effects” that were very similar to our observations. Salt recovered from Hutchinson, Kansas, was heated and found to exhibit violent fracture at approximately 280°C, and the decrepitation temperature did not appear to depend on heating rate. They reported that the explosion was violent enough to lift an oven door and rupture a wire basket that was used to

contain the salt sample being heated. Bradshaw and McClain considered three explanations for the decrepitation including differential thermal expansion, chemical reactions, and pressure effects of brine inclusions. They concluded that the prime cause was likely the increase in pressure resulting from heating the brine inclusions in the salt. Bradshaw and McClain also reported on decrepitation studies performed on salt from several other locations and found that bedded salts tended to exhibit decrepitation at approximately 250°C to 380°C, but no domal salts exhibited any decrepitation even at temperatures up to approximately 400°C. This finding is generally consistent with our observation that the Avery Island domal salt in our testing did not decrepitate even though it was exposed to the same elevated temperatures as the WIPP bedded salt specimens.

RSI-2184-13-009

Figure 8. Posttest Photograph of Specimen WIPP/QGU37-20/2 Rubble.

In summary, the four tests that exhibited violent failure provided useful information about the upper temperature limit for the onset of decrepitation in the WIPP bedded salt. Decreptiation does not represent an unanticipated event. This test matrix purposefully probed temperature boundaries and obviously found them. No decrepitation was observed at a temperature of 250°C, but two of the three tests attempted at 270°C failed. Both tests at temperature targets greater than 270°C failed, so it is apparent that a temperature of approximately 270°C is the upper limit for avoiding violent decrepitation in WIPP salt.

The results of the successful tests are presented using graphs of stress and strain measurements made during the mechanical loading after the specimens had established equilibrium at their target temperature. For all test results, axial strain is derived by first correcting the LVDT measurement for machine softness. Axial strain is calculated as a natural (logarithmic) strain using a sign convention of compression positive. Isochoric deformation is assumed so the lateral strain is estimated as the opposite sign value of one-half the axial strain,

and an updated value for the cross-sectional area of the specimen can be obtained. The current axial stress is then calculated as the ratio of the load cell measurement to the current specimen area.

The results for the successful uniaxial tests are presented in Figures 9, 10, and 11 to represent the three stages of loading: (1) the initial loading at a constant strain rate with unload/reload cycles at 5 percent and 10 percent strain (Figure 9), (2) the stress-relaxation portion of the test that represented the time-dependent behavior (Figure 10), and (3) the final loading to ultimate strength performed at the end of the test (Figure 11).

The initial loading responses shown in Figure 9 demonstrate the expected effect of temperature on the salt deformation. As temperature increases, less stress is required to induce a given level of strain in the specimen (i.e., increases in temperature promote plastic behavior and ductility). The unload/reload cycles at 5 percent and 10 percent strain provided in Figure 9 are typical for salt in that they exhibit very linear (elastic) behavior when the stress is less than whatever maximum stress had preceded the onset of the unloading. The plot ends at an axial strain of 12 percent because that is the strain level where the stress-relaxation portion of the test began. Fits to quantify elastic moduli were made using data from the reload portion of the cycles over a fixed stress interval of 3 MPa to 7 MPa. These fits provided estimates of Young's modulus and those values are listed in Table 4. The values in Table 4 indicate that there is little, if any, effect of strain level on Young's modulus, because there is very little difference between the estimates obtained at 5 percent strain and 10 percent strain. This observation would indicate the deformation is dominated by ductile processes rather than brittle or dilatant behavior. To the contrary, there is a monotonic temperature effect. This can be seen more clearly in Figure 12 where Young's modulus is plotted as a function of test temperature. The temperature effect begins to lessen as the temperature approaches the decrepitation temperature limit (270°C), but, in general, Young's modulus decreases with increases in temperature.

The plots in Figure 10 represent the stress-relaxation stage of the tests where the axial strain was held constant at 12 percent overnight (or longer in some cases) after the initial loading. As expected, the axial stress for any given test decreased in a nonlinear fashion beginning with a high rate of decrease that began to stabilize over a period of nearly a day. It is apparent that temperature has a significant effect on the time-dependent behavior of the salt. The tests performed at higher temperature are approaching asymptotic “steady-state” values that represent lower stress values than the lower temperature tests. There is some variability in the results, as demonstrated by the test at 250°C, which appears to have an initial rate of decrease that is greater than the test at 275°C. However, the overall trend with temperature is evident. Some of the tests were continued for longer than the test plan schedule of approximately 1 day to allow (potentially) further evolution of microstructure that might be evident in posttest petrographic studies that are not part of the scope of this project.

The final loading to determine ultimate strength was performed after the stress-relaxation stage was complete, so the axial strain was 12 percent when loading began, as illustrated in Figure 11. As with the initial loading phase, the effect of temperature on the stress-strain behavior becomes evident. The higher temperatures promote plastic deformation and lower ultimate strengths although the effect of the temperature begins to lessen as the temperature approaches the decrepitation limit of 270°C.

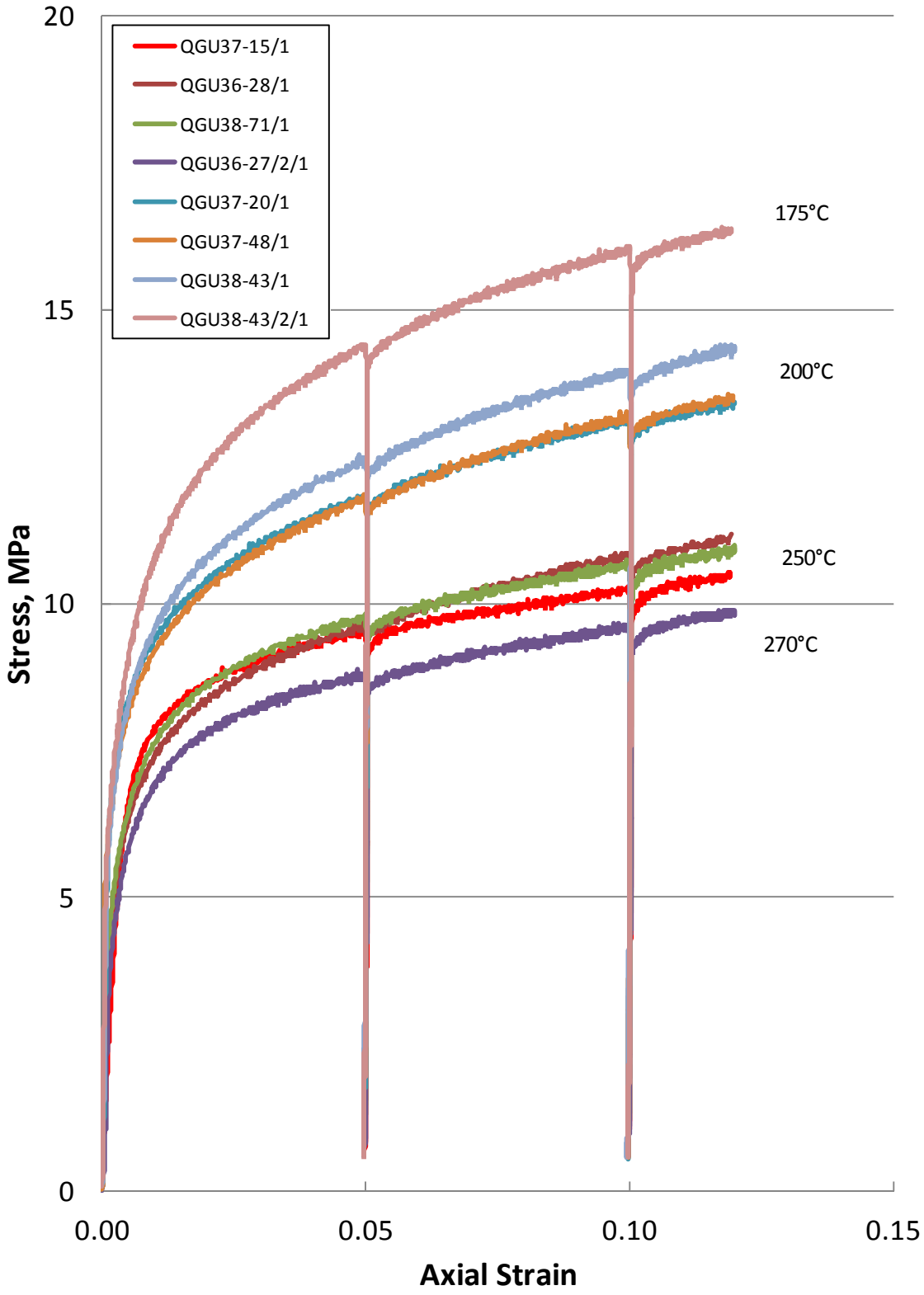

Figure 9. Initial Loading Phase for Uniaxial Tests.

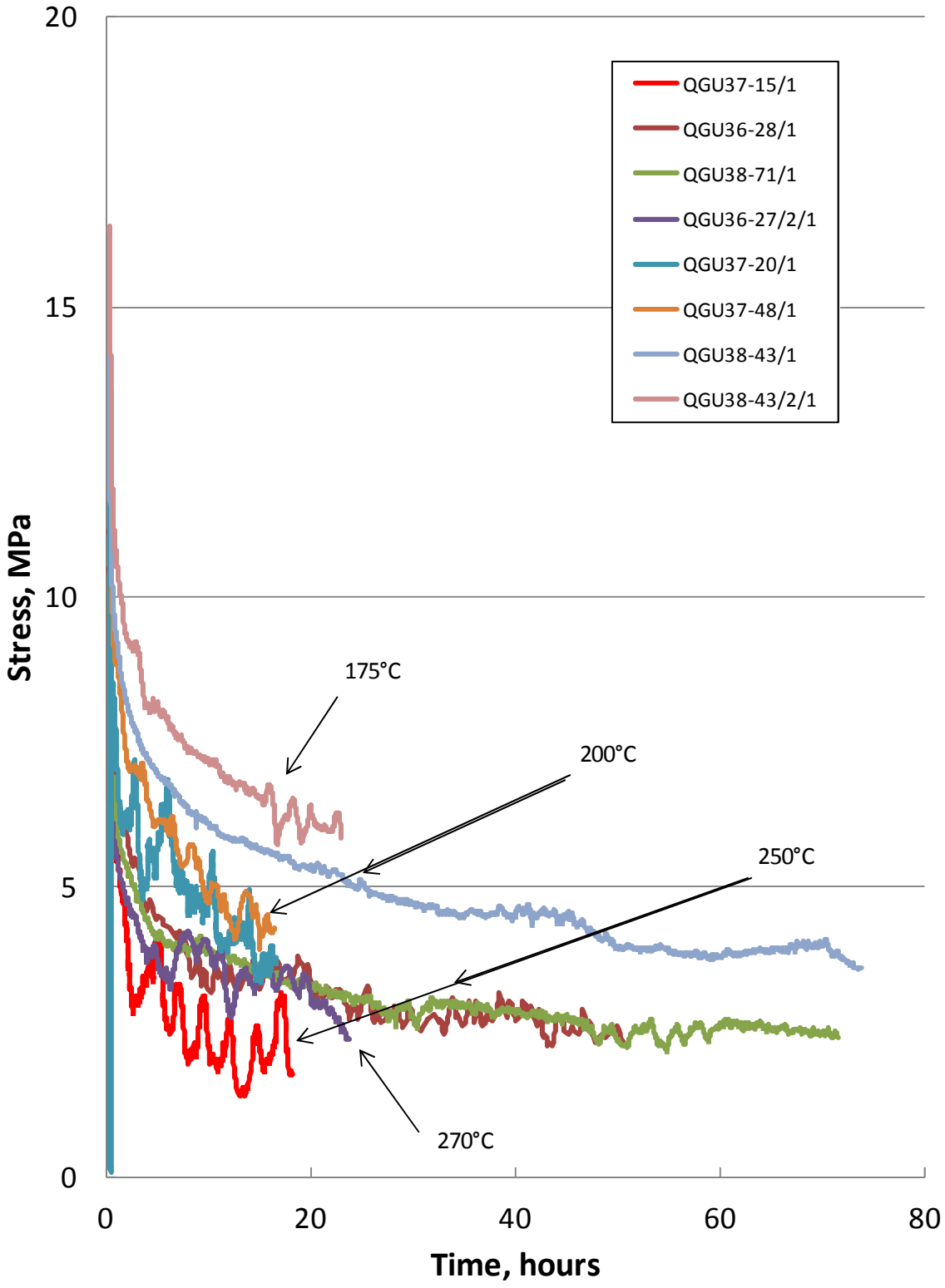

Figure 10. Stress-Relaxation Phase for Uniaxial Tests.

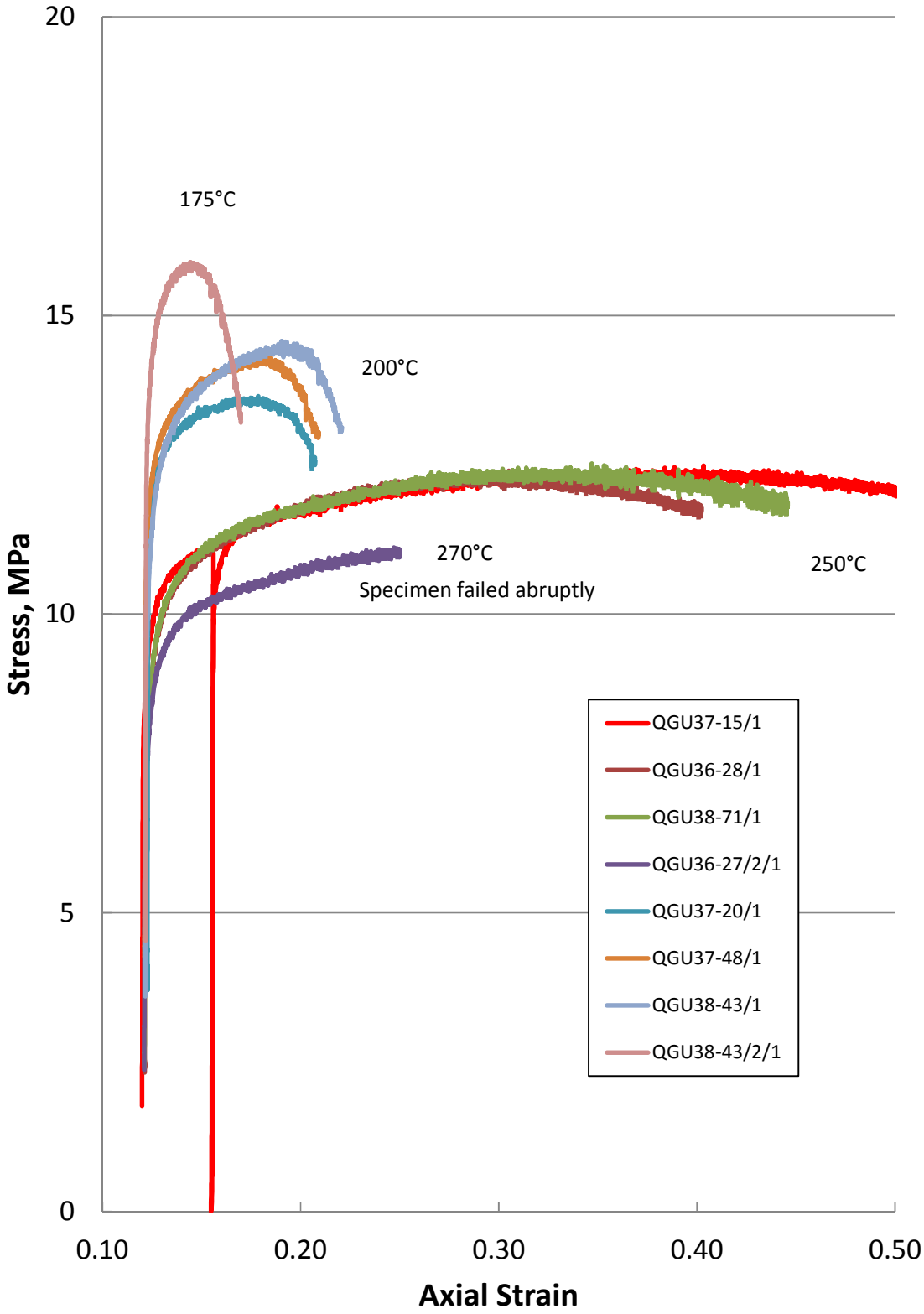

Figure 11. Final Loading Phase for Uniaxial Tests.

Table 4. Estimates of Young's Modulus From Unload/Reload Cycles

Specimen I.D.	Temperature (°C)	Young's Moduli, GPa	
		5% Strain	10% Strain
WIPP/QGU36-27-2/1	270	18.4	18.6
WIPP/QGU37-15/1	250	18.5	18.5
WIPP/QGU36-28/1	250	18.9	19.1
WIPP/QGU38-71/1	250	19.3	18.6
WIPP/QGU37-20/1	200	19.8	18.8
WIPP/QGU37-48/1	200	18.6	19.1
WIPP/QGU38-43/1	200	18.8	18.2
WIPP/QGU38-43-2/1	175	22.3	21.8

Some general comments about the test results: (1) Young's modulus tends to decrease with an increase in temperature; (2) at higher temperature, less stress is required to induce specific strain levels; (3) ultimate strength decreases with an increase in temperature; and (4) the strain at ultimate strength increases with an increase in temperature. All of these monotonic results are consistent with expectations and hypotheses of thermally driven processes. We note the temperature influence on elastic modulus is relatively modest (modulus at room temperature is nominally 30 GPa). The specimens sustained extremely high deformations consistent with isochoric plastic deformational processes. Macroscopic vertical cracks eventually became evident by the time the tests were terminated. The posttest appearance of two of the specimens is displayed in the photographs provided in Figures 13 and 14.

CONSTITUTIVE MODEL EVALUATION

The relatively large database created by this project can provide some sense of the degree of uncertainty one might expect in the high-temperature regime. Additionally, the new tests extend the range of test results for WIPP salt, because the highest temperature used in prior laboratory investigations was 200°C. The question that remains is whether or not existing constitutive models for WIPP salt, based on historical test programs executed at lower temperatures, are capable of predicting these new test results at high temperatures. This question was addressed by making predictions of high-temperature test results using the WIPP salt parameters already defined in the literature and accepted for use in modeling field studies at WIPP [Munson et al., 1989]. The calculations were performed using the RESPEC finite element software package **SPECTROM-32** [Callahan et al., 1989]. The first two phases of a test were modeled (initial loading and stress relaxation) and the model predictions are shown in Figures 15 and 16, respectively. The two figures are the same figures (Figures 9 and 10) presented earlier with the model predictions overlain on the data. The model predictions were performed for temperatures of 200°C and 250°C, and the comparisons are encouraging. The

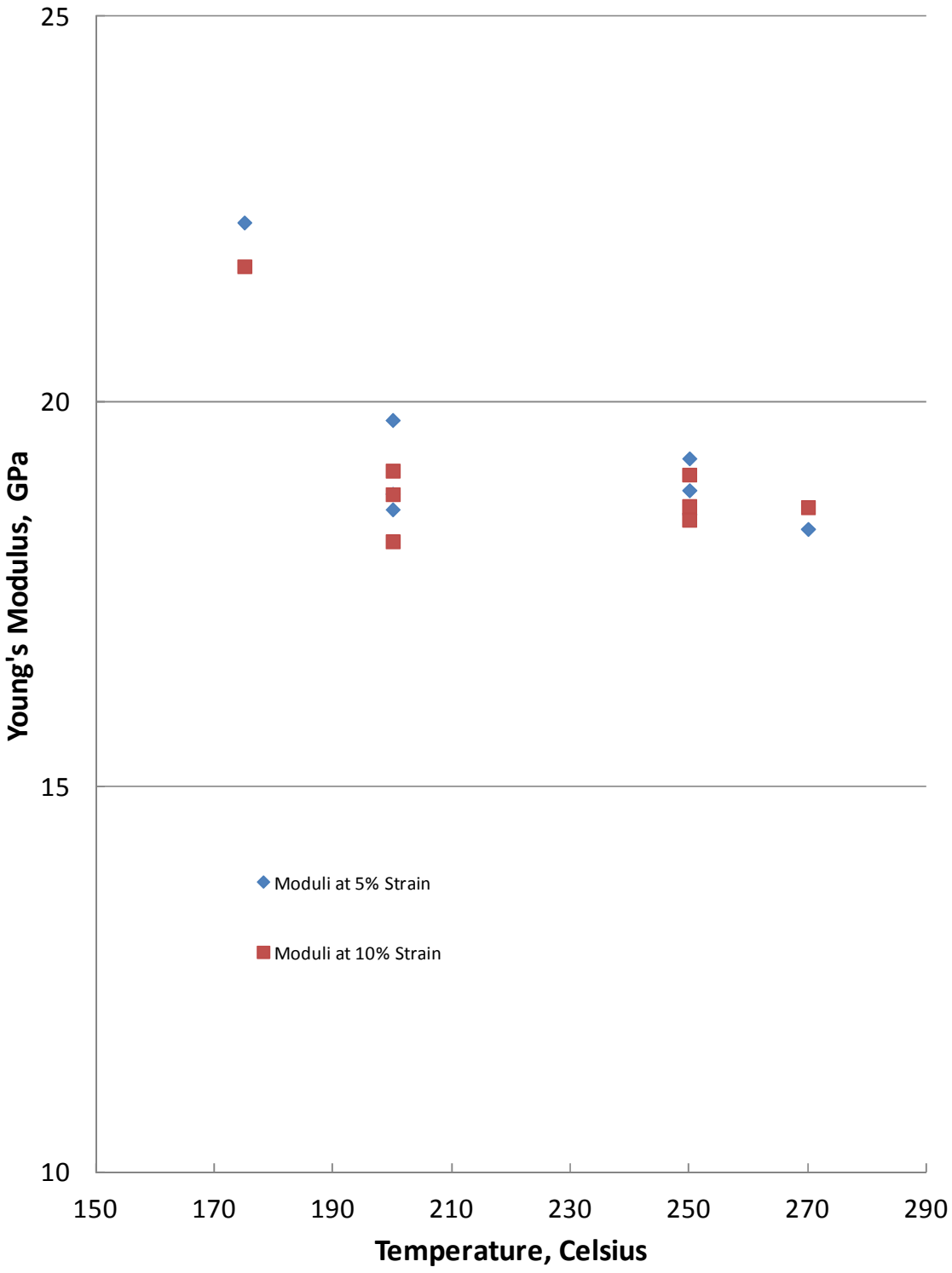

Figure 12. Young's Modulus as a Function of Temperature for WIPP Salt.

Figure 13. Posttest Photograph of Specimen WIPP/QGU37-20/1 Tested at 200°C.

Figure 14. Posttest Photograph of Specimen WIPP/QGU37-15/1 Tested at 250°C.

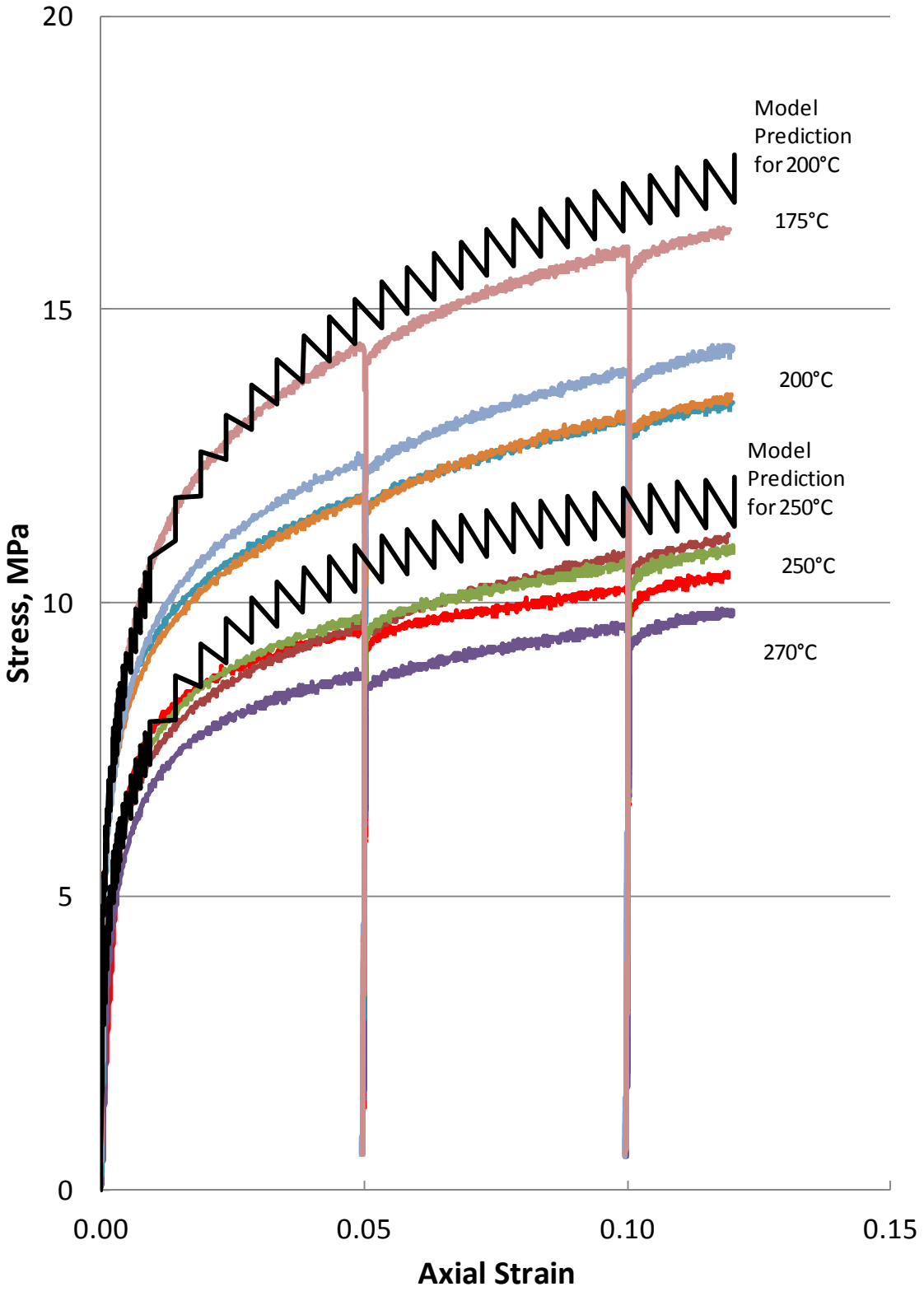

Figure 15. Comparison of Model Predictions and Test Results for Quasi-static Loading.

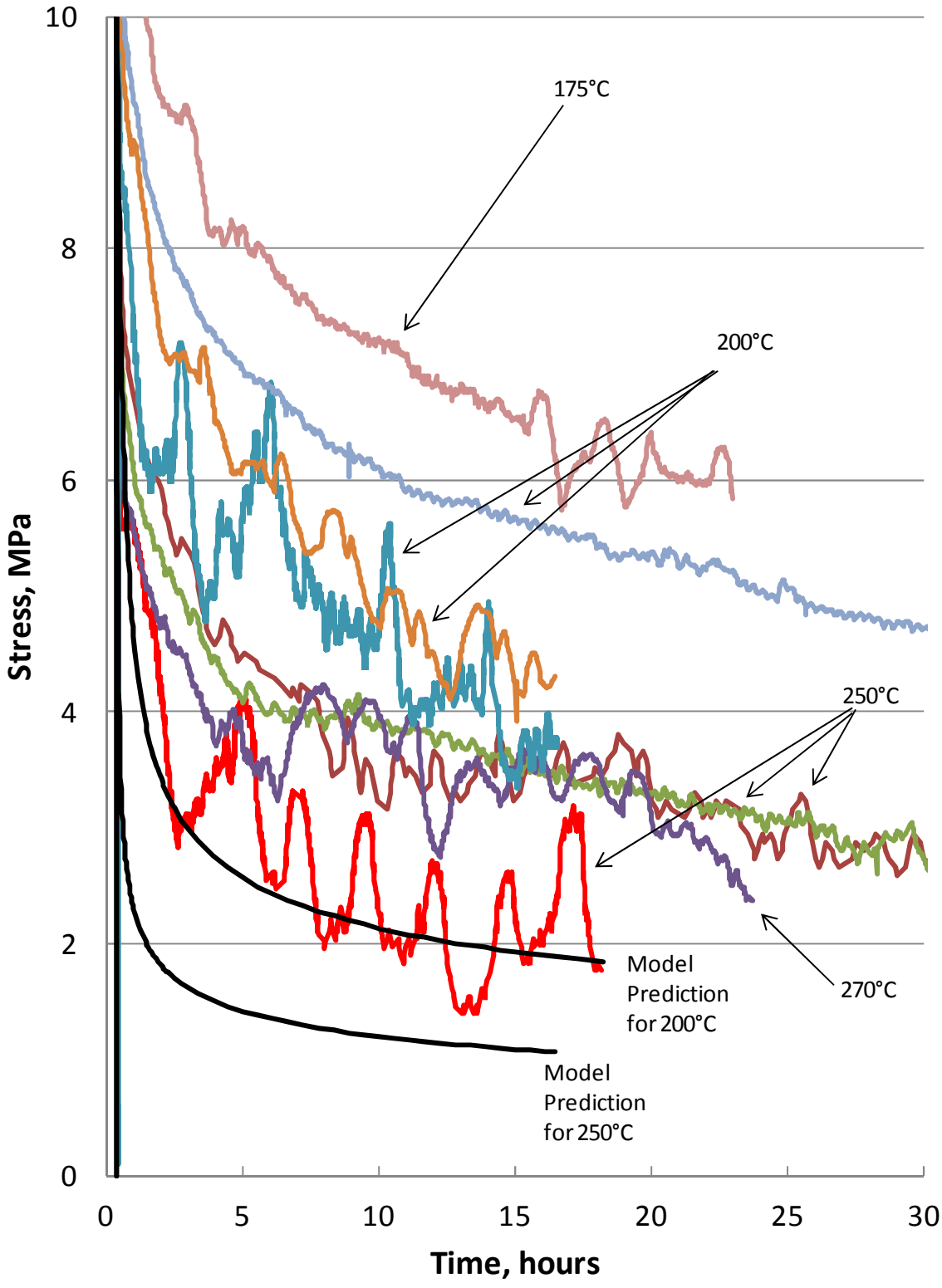

Figure 16. Comparison of Model Predictions and Test Results for Stress Relaxation.

models produced reasonable predictions of the behavior seen at these high temperatures, which means the existing model equipped with existing parameters can reasonably extrapolate to temperatures near the decrepitation limit and provide useful predictions of WIPP salt behavior.

It should be noted here that model predictions were not part of the identified scope of work, nor were these predictions required by the contract. Other research is addressing the larger framework of benchmarking computational capabilities and constitutive modeling. This new research provides an opportunistic preview of modeling high-temperature salt deformation.

REFERENCES

Bradshaw, R. L. and W. C. McClain, 1971. *Project Salt Vault: A Demonstration of the Disposal of High Activity Solidified Wastes in Underground Salt Mines*, ORNL-4555 prepared by Oak Ridge National Laboratory for the U.S. Atomic Energy Commission

Callahan, G. D., A. F. Fossum, and D. K. Svalstad, 1989. *Documentation of SPECTROM-32: A Finite Element Thermomechanical Stress Analysis Program*, DOE/CH/10378-2, prepared by RE/SPEC Inc., Rapid City, SD, for the U.S. Department of Energy, Chicago Operations Office, Argonne, IL, Vols. I and II.

Mellegard, K. D., 2013. *Elevated Temperature Unconfined Compression Tests on Salt*, Test Plan SNL-FCT-TP-13-0001, prepared for Sandia National Laboratories Fuel Cycle Technology Program, Sandia National Laboratories, Albuquerque, NM.

Mellegard, K. D., 2012. *Initial Laboratory Unconfined Compression Uniaxial Stress Test Results on Salt Specimens From the Waste Isolation Pilot Plant*, Technical Letter Memorandum RSI/TLM-185, submitted to F. D. Hansen, Sandia National Laboratories, Albuquerque, NM, by K. D. Mellegard, RESPEC, Rapid City, SD, September.

Mellegard, K. D., G. D. Callahan, and F. D. Hansen, 2013. "High-Temperature Characterization of Bedded Permian Salt," SAND2013-4040J, ARMA 13-303, *Proceedings, 46th U.S. Rock Mechanics/Geomechanics Symposium*, San Francisco, CA, June 23–26, CD-ROM.

Munson, D. E., A. F. Fossum, and P. E. Senseny, 1989. *Advances in Resolution of Discrepancies Between Predicted and Measured In Situ WIPP Room Closures*, RSI-0347, SAND88-2948, for Sandia National Laboratories, Albuquerque, NM, March.

KDM:llf

ATTACHMENT A

GEOLOGIC CORE DESCRIPTION

Dennis W. Powers, Ph. D.

Consulting Geologist

March 12, 2001

Terry MacDonald and Frank Hansen
Sandia National Laboratories-Carlsbad
4100 National Parks Highway
Carlsbad, NM 88220

Dear Terry and Frank:
Here is an interim summary of features and proposed activities regarding the 5 cores from the Disturbed Rock Zone I re-examined last week. These descriptions are subject to revision in the final report now in preparation.

QGU 12

Core was taken at about the contact between MU 4 & 5. It shows extensive subhorizontal clay laminae that developed in "salt saucers" at the depositional surface, and the core samples what would commonly be called "clay f".

Fractures were only observed within 0.3 ft of the rib face, but they have the largest aperture of any fractures. There may have been salt plucking or clay erosion by air flow during drilling.

At about 0.4 ft depth, brown clay displays slickensides @ an angle of about 45° from vertical, with the lower end of the slickensides closer to the rib face and upper end downhole. I suggest these slickensides are more likely depositional (pedogenic) than structural, but there is no way to be certain.

There is no observed strain beyond a depth of about 0.3 ft. It seems likely that the clay is absorbing strain with no visible effects, and the halite is not subject to sufficient stress within this regime to develop features observed in halite rock without significant clay.

Recommended program: photograph unwrapped core from 0-4.5 ft at close range from a side view; slab from 0-4.3 ft along vertical axis to see fractures and depositional features; make one cut ⊥ to the core axis at about 4.4 ft to display clay textures; re-examine, re-photograph, and re-describe slab as appropriate.

QGU 36

Core was taken in the lower part of MU 3. It shows coarse clear halite with few impurities.

Halite grains appear to be elongate (l:w is ~ 2:1) along a plane parallel to the rib wall due to fracturing across crystals. Strain planes due to these fractures are parallel to the rib wall near the wall, with the angle to the long core axis increasing beyond about 2.8 ft. At about 4.8 ft, strain planes are ⊥ to the long core axis, and they become more abundant beyond about 6.5 ft. Fractures in this core have no macroscopically measurable aperture.

Core breaks are parallel to the rib face near the wall; beyond about 4.8 ft, breaks tend to be ⊥ to long core axis. Break spacing is ~ 1 ft to depth of 9 ft, then is shorter to TD.

140 Hemley, Anthony, TX 79821
Telephone: (915) 877-3929 E-mail: dwpowers@htg.net *FAX: (915) 877-5071*

The breaks on this core, especially near the rib face, show cleavage control as follows:

- coarse crystals (> ~ 1 inch) tend to break along the cleavage face closest to the plane of the strain fabric;
- smaller crystals tend to break along a series of close-stepped cleavages along the 2 cleavage planes where the average of these 2 planes is close to the plane of the strain fabric. The close-stepped cleavages generally appear macroscopically to have cleavage face widths in ratios between about 1:1 and 2:1.
- There are only a few instances of conchoidal to hackly fracture on these crystals.

Recommended program: Close-range photographs with scale of top, bottom, and one side of the core to show fabrics; slab along horizontal plane full length of core; re-examine and re-describe as appropriate; photograph one side of slab at close range.

QGU 37

This core has similar geology to QGU 36 and 38. It was drilled in the alcove corner.

Strain planes in this core are all ⊥ to the long axis of the core. This core is much more disked than 36 or 38 to a depth of about 14.5 ft. Beyond that depth, the core generally is in lengths of 6 inches to 1 ft. In addition, core breaks near the rib wall show a convex face on the core end nearest the rib and a fitted concave face downhole.

The crystal relief on the core breaks of QGU 37 appears to be less than that on 36. In addition, the crystals appear to have more hackly or conchoidal surfaces, few large cleavages, and very common stepped cleavage with curvature.

I suggest that the greater disking in the first 15 ft, strain planes ⊥ to the long core axis, and convex/concave breaks near the rib face are all a consequence of the location at the corner of the Q Room Alcove. It seems to me that the stress is likely to be concentrated more tightly near the corner than along the planar face and may account for all these features. I wonder if this may also account for the apparent greater fracturing rather than cleavage control on core break surfaces.

Recommended program: none at this time. May be useful to slab the first 2 ft along horizontal plane later to compare dislocation densities.

QGU 38

The geology of this core is similar to 36 and 37.

There are many similarities between 36 and 38 in fabric, as the crystals again show strain planes parallel to the rib face near the rib face. These strain planes are no longer observable beyond 4.5 ft. Strain planes ⊥ to the core axis are apparent from about 3.6 ft, co-existing with the angled strain planes.

Disking becomes much more intense from about 4.5 to 11 ft, and strain planes ⊥ to the core axis are faint or not observable beyond about 10 ft.

Recommended program: Close-range photographs with scale of the core from the top and one side from 0 to TD where core pieces are larger than about 4 inches; slabb from 0 - 4.5 ft along horizontal plane (?after results of QGU 36 are available).

QGU 39

QGU 39 was cored in the upper middle part of MU 0, at the point where clay content is beginning to increase vertically. Much of the first 7 ft of the core was taken along the edge of a dissolution pipe and shows the lateral transition between finer opaque halite to coarse clear halite, sometimes with clay concentrations along this boundary.

The core shows some of the same fabric parallel to the rib face that is observed in QGU 36 and 38. The "foliation" angle to the long axis of the core begins to increase at about 3 ft and is not discernible beyond about 3.3 ft depth.

Several fractures with discernible aperture are located at 0.75, 0.80, and 1.25 ft, and these fractures tend to parallel the rib face. Core breaks are ⊥ to the long core axis, and the rock quality is generally good in this core. There are short intervals of disking.

Recommended program: close-range photos with scale of top and one side of total core prior to slabbing; slab from rib face to about 7 ft along horizontal plane; examine slabs; redescribe and rephotograph as appropriate; make vertical cut ⊥ to long core axis at 7.4 ft to show clay/halite relationships and possible clay illuviation.

Priorities

From the recommendations above, the first priority is QGU 36, mainly because it is the core that shows the most interesting features and is well-preserved. From it, better ideas can be derived of the significant features to check on other cores.

I think the second and third priorities are the more limited items on QGU 39 and 38, probably in that order. Additional slabbing, to greater depths, may be considered if the dislocation densities begin to show patterns of interest or if other features of interest develop.

The last priority right now is probably QGU 12. Although it is interesting sedimentologically, there is very limited macroscopic evidence of strain in the DRZ (~ 0 - 0.3 ft). It will certainly be useful to compare a core like this from high on the rib face to those in the middle (QGU 36, 38) and lower part (QGU 39).

Please circulate these preliminary results as you see appropriate to develop consensus on the next steps in relating strain features to the DRZ and its properties. I am working on a report that will provide more detail of these observations.

Sincerely,

electonic file without signature

Dennis W. Powers

ATTACHMENT B

AMERICAN ROCK MECHANICS PUBLICATION
ARMA 13-303, SAND2013-4040J

ARMA 13-303

High-temperature characterization of bedded Permian salt

Mellegard, K.D. and Callahan, G.D.
RESPEC, Rapid City, South Dakota, USA
Hansen, F.D.
Sandia National Laboratories, Albuquerque, New Mexico, USA

This paper was prepared for presentation at the 47th US Rock Mechanics / Geomechanics Symposium held in San Francisco, CA, USA, 23-26 June 2013.

ABSTRACT: Generic salt research and development sponsored by the Department of Energy includes uniaxial testing of bedded salt to 300°C. A suite of such testing was put forward as one of the prerequisite efforts for advancing the studies of heat-generating waste in salt. Precise loading was applied while each specimen was very accurately heated inside an environmental chamber. These reconnaissance tests extend the considerable database available for Permian-bedded salt. Most of these tests were developed during site characterization for the Waste Isolation Pilot Plant. These laboratory studies examine temperature effects on elastic properties, time-dependent creep behavior, and ultimate strength in an unconfined condition. Posttest microstructural observations allow assessment of deformational processes. Fluid inclusions create vast differences in behavior between bedded and domal salt at high temperatures including a propensity for bedded salt to violently decrepitate at temperatures near 280°C while domal salt remains stable to 300°C. The test data developed for this paper provide an initial evaluation of how well the existing constitutive model extrapolates to temperatures outside of the substantial database at much lower temperatures and provides an indication of the model validity in the high temperature regimes.

1. INTRODUCTION

A repository for heat-generative nuclear waste provides an engineering challenge far beyond general experience. The long-term requirements of repository performance are precluded from direct observation and, therefore, must be predicted. Accurately predicting a repository response can only be done through applying valid models. In the instance of a salt formation providing the host medium, the scientific community has made great strides toward formulating and using structural codes that capture the observed physical phenomena. For example, strain rates are cast as functions of stress difference, temperature, and structure because salt deformation subjected to expected repository conditions has been shown to be very sensitive to temperature and stress. Other studies show that history effects, normal transient response (where strain rate decreases), inverse transients (where strain rate increases), and the dependence of creep rate on stress difference and temperature are a direct consequence of existing and evolving substructures.

One aspect of this paper involves reporting on high-temperature uniaxial laboratory tests performed on salt recovered from the Waste Isolation Pilot Plant (WIPP) facility in Carlsbad, New Mexico. Tests performed at 200°C overlap with historical databases and provide a point where predictive models based on those databases can be checked for the current work. The test results at temperatures above 200°C provide new data so that extrapolation outside the actual test database will not be necessary. Some waste packages could possibly involve temperatures greater than 200°C, so this high-temperature research will help with designing and evaluating such disposal concepts.

The laboratory results generated in the tests described here are compared to predictions of the deformation (before the tests were run) that were obtained using a finite element software package that integrates a constitutive model for the WIPP salt. A viable constitutive law should provide a reasonable approximation of laboratory results and reflect the physical processes that account for deformation. An extension of empirical results provides one indication of the existing model adequacy. Observational microscopy will document the micromechanical processes to evaluate their consistency with the basis of the model. Together, the model results, the predictions using the existing model, and the substantiation of the microprocesses provide a sound scientific basis for extrapolating the model to temperatures that have not been experienced in the laboratory before.

2. SPECIMENS

2.1. Core Sample Recovery

The salt core tested in this program was provided by Sandia National Laboratory (SNL) and were recovered from the WIPP site near Carlsbad, New Mexico. The core recovery locations were horizontal boreholes drilled for the Disturbed Rock Zone (DRZ) Characterization Test Plan at the WIPP. The sources of core were three boreholes identified as QGU36, QGU37, and QGU38.

SNL performed a limited petrographic analysis on the salt core recovered from the boreholes. The result of primary interest for the current uniaxial testing is the conclusion that the core samples from the three boreholes were considered to have few impurities, and the geology was similar among all three boreholes.

2.2. Specimen Preparation

Testable specimens were prepared by first sawing a piece of salt core to an approximate length-to-diameter ratio of L:D=2. The walls and ends of the cylinder were then machined in a horizontal lathe to produce a finished, right-circular cylinder whose ends were flat, parallel, and perpendicular to the specimen's sides. A typical machining setup is depicted in Figure 1, and the carbide tooling is visible next to the specimen surface. The finished specimens were then measured to determine their length and diameter. They were also weighed, and a bulk density was calculated using the specimen's dimensions to determine volume. A summary of the testable specimens that were prepared is presented in Table 1. The bulk density values are very uniform and very near the typical value for halite (2.15 grams per cubic centimeter [g/cc]). This supports the previously referenced geological assessment that the specimens were relatively free of impurities.

Fig. 1. Typical horizontal lathe machining setup for preparing cylindrical specimens.

During the machining process that finished the core in a horizontal lathe, the cutting tool frequently encountered fluid inclusion brine as the circumferences of the cylinders were trimmed to a final dimension. Even though the core appeared to be dry on the surface when it was initially mounted in the lathe, wet spots began to appear when the cutting tool proceeded to make repeated small machining passes (reducing the radius by only approximately 0.3 millimeter [mm] per pass). This was evidence of non-interconnected brine inclusions. The number of inclusions appeared to increase with cutting depth, but they were observed even during the first pass. This indicates that some isolated brine inclusions existed within approximately 0.3 mm of the specimen surface. A photograph of a newly machined specimen is shown in Figure 2, and the wet brine spots are visible as dark round circles scattered on the surface of the specimen.

Table 1. Summary of fabricated salt specimens

Specimen I.D.	L (mm)	D (mm)	Mass (g)	ρ (g/cc)
WIPP/QGU37-20/1	204.13	90.97	2,859.60	2.16
WIPP/QGU37-20/2	207.32	90.96	2,908.50	2.16
WIPP/QGU37-15/1	205.34	89.74	2,809.40	2.16
WIPP/QGU37-45/1	206.59	91.03	2,903.70	2.16
WIPP/QGU36-17/1	204.04	89.53	2,776.60	2.16
WIPP/QGU36-18/1	204.87	89.59	2,786.35	2.16
WIPP/QGU36-27-2/1	206.76	89.39	2,791.95	2.15
WIPP/QGU36-28/1	206.12	89.51	2,792.55	2.15
WIPP/QGU37-48/1	206.54	89.53	2,798.40	2.15
WIPP/QGU37-48/2	207.88	89.56	2,820.40	2.15
WIPP/QGU38-43/1	206.98	89.59	2,816.85	2.16
WIPP/QGU38-43-2/1	207.71	89.43	2,820.55	2.16
WIPP/QGU38-71/1	207.23	89.54	2,820.80	2.16

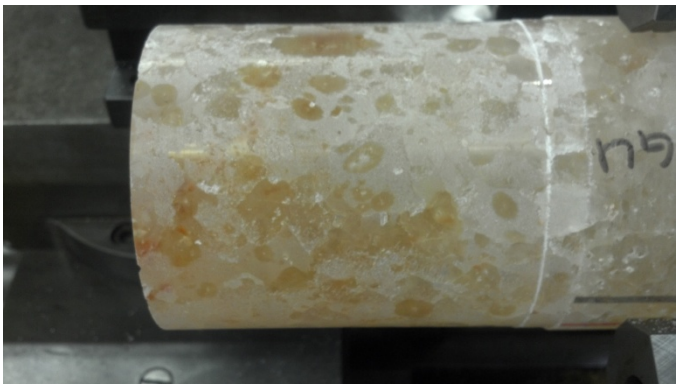

Fig. 2. Waste Isolation Pilot Plant salt specimen brine inclusions (darker ovoid areas are wet).

3. UNIAXIAL TESTING

3.1. Procedure and Equipment

The testing was completed using a universal test system with four reaction columns referred to as the UTS4 system. The UTS4 is a computer-controlled, servo-hydraulic system manufactured by MTS Systems of Eden Prairie, Minnesota. The computer controls the loading in two modes: a stress rate mode using the load

cell output as a feedback signal, or a strain-rate mode that uses a Linear Variable Differential Transformer (LVDT) output to control loading. An environmental chamber is mounted in the test system to provide the high-temperature environment required to perform unconfined tests at temperatures up to 300°C.

A photograph of the test system is provided in Figure 3. The photograph illustrates the environmental chamber mounted in the test frame with the chamber door open for easy viewing of its interior. Two salt specimens are inside the chamber. The specimen on the left is an Avery Island domal salt specimen instrumented with thermocouples to monitor salt specimen temperatures. Some other thermocouples suspended in air monitor the temperature of the air inside the chamber. Located in the load train in the middle of the chamber is a tested salt specimen (somewhat barrel shaped). Above and below the specimen are steel loading platens attached to long insulating rods that provide insulation between the hot specimen inside the chamber and the loading actuators outside the chamber. Just in view at the top of the photograph is the load cell that monitors axial loading force. An LVDT that monitors axial displacement is mounted inside the hydraulic actuator at the base of the system (not in view).

Fig. 3. UTS4 uniaxial test system equipped with high-temperature environmental chamber.

All three sets of instrumentation, including the load cell, the LVDT, and the thermocouples, were calibrated against in-house standards that are certified and traceable to National Institute of Standards and Technology (NIST) references. Calibration records indicate that the load cell force readings and the LVDT displacement measurements are accurate to within ± 1% of reading, and the thermocouple temperatures are accurate to within ± 2°C. Because the LVDT measures total axial displacement including some nonspecimen contributions, a "machine softness" factor that allowed the correction of the LVDT measurements was determined.

The test procedure was based on the assumption that the internal structure of a specimen is directly correlated to the measured axial strain and strain rate. This assumption implies that strain-controlled load paths would be beneficial, because changes in load levels could be performed at the same strain levels in each test. In this case, specimen microstructure would all be at the same "state" when the loads were changed.

The test procedure first involved bringing the specimen to the desired temperature and then applying a three-stage load path. The load path stages included the following:

- Stage 1: Initial loading was performed at a constant strain rate of $10^{-4}s^{-1}$ with pauses at strain levels of 5%, 10%, and 12%. At 5% and 10% strain, unload/reload cycles were performed to generate data that could be used to estimate Young's modulus. The loading pause at 12% strain was used to initiate the next stage.
- Stage 2: The second stage of loading began when the constant strain-rate loading was suspended at an axial strain of 12%. The strain rate was reduced to zero and a stress relaxation stage began where the strain level was maintained at 12% overnight (at least 16 hours).
- Stage 3: The final stage was a return to constant strain-rate loading following the stress relaxation phase. In this final stage, the loading was continued to determine ultimate strength.

3.2. Test Results

A total of four uniaxial tests were attempted—two at 300°C, one at 200°C, and one at 250°C. The two tests at 300°C were unsuccessful because the specimen decrepitated at temperatures less than 300°C. The tests at 200°C and 250°C were completed successfully. The test matrix is summarized in Table 2.

Table 2. Test matrix summary

Specimen I.D.	Temp (°C)	Status
QGU37-20/1	200	Successful
QGU37-15/1	250	Successful
QGU37-20/2	300	Decrepitated at 280°C
QGU37-45/1	300	Decrepitated at 285°C

The two tests attempted at 300°C were similar because both of them exhibited a violent decrepitation as the specimen temperature (estimated by thermocouples located along the central axis of the Avery Island salt specimen collocated in the test chamber) reached approximately 280°C and no mechanical loading could be applied. Thus, stress and strain data are not available for these tests. However, some observations can be made about how the decrepitation apparently did not depend on the rate of heating. For example, specimen WIPP/QGU37-20/2 was placed in the environmental chamber, and the chamber temperature was ramped to

300°C at a rate of 1°C/minute. Decrepitation occurred at approximately 280°C with a violent explosion that reduced the specimen to rubble.

Anticipating that the heating rate might have been too fast, the next specimen, WIPP/QGU37-45/1, was heated to just 250°C at a rate of 1°C/minute and then allowed to remain at 250°C for 24 hours. After 24 hours, the test chamber temperature was ramped to 300°C at a rate of 1°C/minute. When the specimen temperature reached 285°C (indicated by the thermocouples in the Avery Island specimen), a violent decrepitation caused the top third of the specimen to explode into rubble. At that point, the heat was turned off, but approximately 5 minutes later, the remaining two-thirds of the specimen also exploded and effectively reduced the entire specimen to rubble.

A posttest photograph, shown in Figure 4, is typical of the rubble that remains after the violent decrepitation occurs. Note in Figure 4 that the Avery Island domal salt specimen still remained intact throughout both attempts at 300°C tests on the WIPP salt. The vast difference in salt response at 280°C is attributed to fluid inclusions. Figure 5 includes two photomicrographs of the natural presence of fluid inclusions in bedded salt. The highly magnified image in the upper right exemplifies the galaxies of fluid inclusions ranging in size from 5 mm to microns in a typical bedded salt. The second image in Figure 5 captures the motion of internal fluid inclusions as the grain is highly deformed (in this case, at 250°C). Fluid inclusions tend to collect along the tight grain boundaries, which might be expected as the fluid itself promotes the creation of the grain boundary. Although fluid inclusions are a minor constituent of the total brine present in bedded salt, they give rise to effects at high temperatures including decrepitation and fluid-assisted grain boundary migration [1].

Fig. 4. Posttest photograph of rubble of specimen WIPP/QGU37-20/2.

The violent decrepitation observed in the two tests at 300°C is not unique to WIPP salt. Similar observations were made during the Project Salt Vault [2] investigation in Lyons, Kansas. They reported observations characterized as “trapped moisture effects” that were very similar to our observations. Salt recovered from Hutchinson, Kansas, was heated and found to exhibit violent fracture at approximately 280°C, and the decrepitation temperature did not appear to depend on the heating rate. They reported that the explosion was violent enough to lift the oven door and rupture the wire basket that was used to contain the salt sample being heated. The Project Salt Vault study considered three explanations for the decrepitation including differential thermal expansion, chemical reactions, and the pressure effects of brine inclusions. They concluded that the prime cause was likely the increase in pressure resulting from heating the brine inclusions in the salt. They also reported on decrepitation studies performed on salt from several other locations and found that bedded salts tended to exhibit decrepitation at approximately 250°C to 380°C, but domal salts did not exhibit any decrepitation, even at temperatures up to approximately 400°C. Domal salt has few fluid inclusions and much lower total brine content than bedded salt. This finding is generally consistent with our observation that the Avery Island domal salt in our testing did not decrepitate, even though it was exposed to the same elevated temperatures as the WIPP bedded salt specimens.

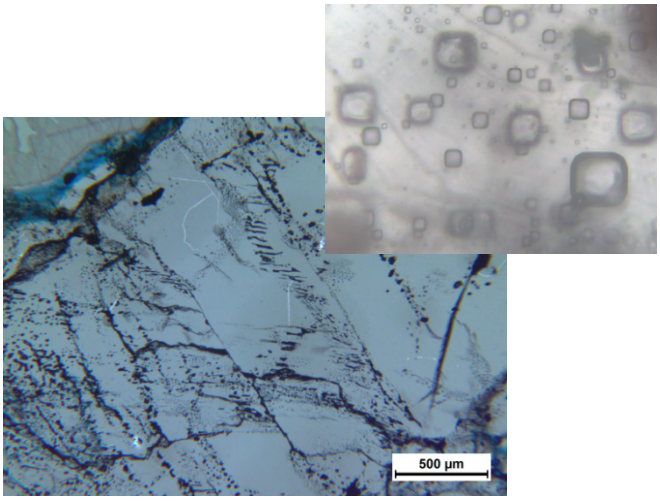

Fig. 5. Deformed and undeformed fluid inclusions in bedded salt.

The uniaxial tests at 200°C and 250°C were successful, and the results of those tests are presented using graphs of stress and strain measurements made during the mechanical loadings after the specimens had established equilibrium at their specified temperature. For all test results, the axial strain is derived by first correcting the LVDT measurement for machine softness and then using the corrected LVDT displacement value to determine the current specimen length. Axial strain is then calculated as the natural logarithm of the ratio of the current specimen length to the original specimen length (using a sign convention of compression positive). Isochoric deformation is assumed, so the lateral strain is estimated as the opposite sign value of one half the axial strain, and an updated value for the cross-sectional area of the

specimen can be obtained. Then, the current axial stress is calculated as the ratio of the load cell measurement to the current specimen area.

The test results for the uniaxial test at 200°C are presented in Figures 6, 7, and 8, which are plots of the overall test history, the unload/reload cycles at the beginning of the test, and the final loading to ultimate strength performed at the end of the test, respectively.

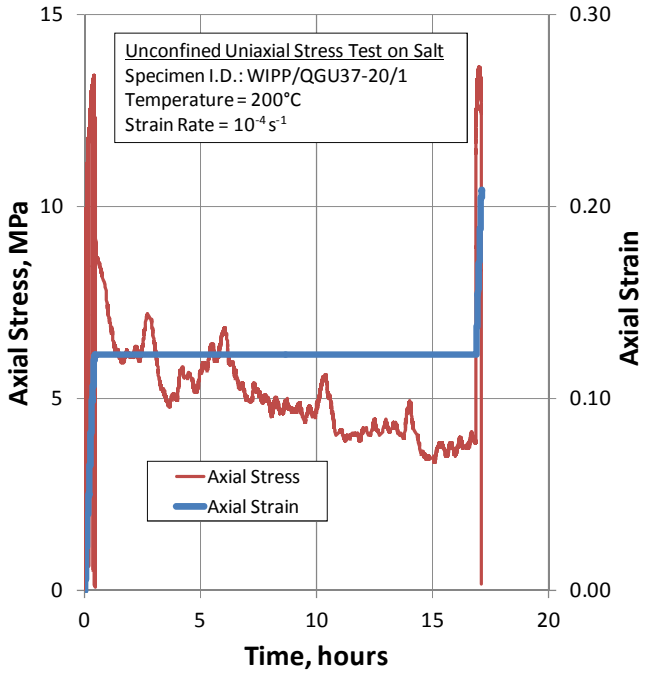

Fig. 6. Complete test history for uniaxial test on specimen WIPP/QGU37-20/1 at 200°C.

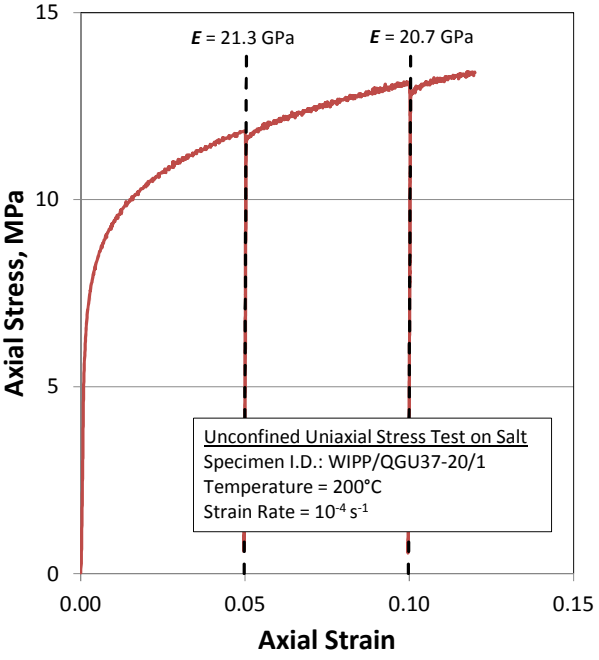

Fig. 7. Unload/reload cycles on specimen WIPP/QGU37-20/1 at 200°C.

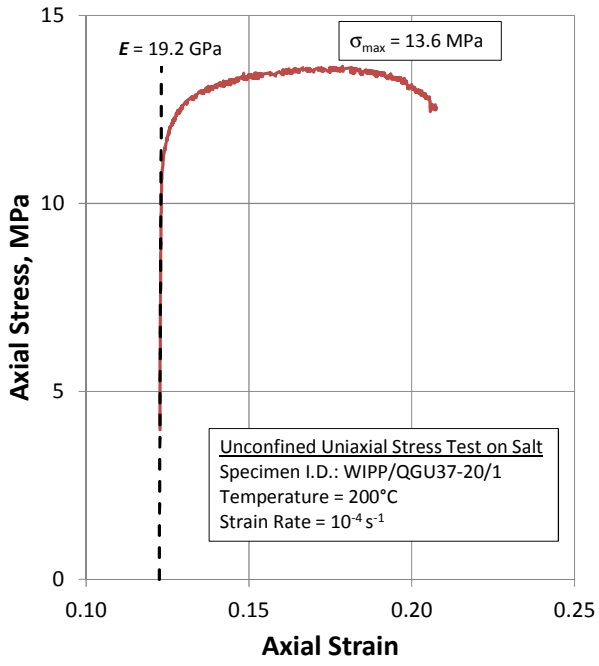

Fig. 8. Final loading to ultimate strength for specimen WIPP/QGU37-20/1 at 200°C.

The plots in Figure 6 are dominated by the stress-relaxation stage of the test where the axial strain was held constant at 12% overnight after the initial loading. As expected, the axial stress decreased substantially and began to stabilize at near 4 MPa before initiating the final loading to determine the ultimate strength. The stress relaxation exhibited a cyclic response, which might indicate some inconsistency in the real-time calculation of stress and strain during the interval. Further investigation of this phenomenon will ensue in the next stages of these investigations.

The unload/reload cycles provided in Figure 7 are typical for salt because they exhibit very linear (elastic) behavior when the stress is less than the maximum stress achieved before unloading. Fits to the linear interval of the reload portion of the cycles provide estimates of Young's modulus, and those values are shown on the plot. The plot ends at an axial strain of 12%, because that is the strain level where the stress-relaxation portion of the test began. The Young's modulus fits indicate that there might be some small effect of the strain level on the elastic constants, because the fitted value at a strain of 10% is slightly smaller than the value estimated at a strain of 5%. The final loading to determine the ultimate strength was performed after the stress-relaxation stage was complete, so the axial strain was 12% when loading began, as illustrated in Figure 8. An ultimate axial stress of 13.6 MPa was clearly defined because loading was continued until the specimen began to lose its ability to sustain further increases in axial stress, and it actually began to exhibit some postpeak weakening. Most of the damage probably accumulated during this last test phase.

The test results for the uniaxial test at 250°C are presented in Figures 9, 10, and 11, which are plots of the overall test history, the unload/reload cycles at the beginning of the test, and the final loading to the ultimate strength performed at the end of the test, respectively.

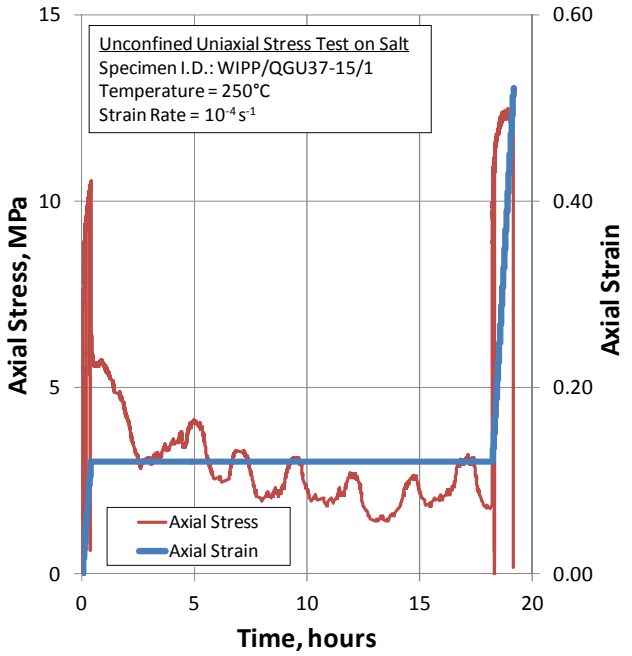

Fig. 9. Complete test history for uniaxial test on specimen WIPP/QGU37-15/1 at 250°C.

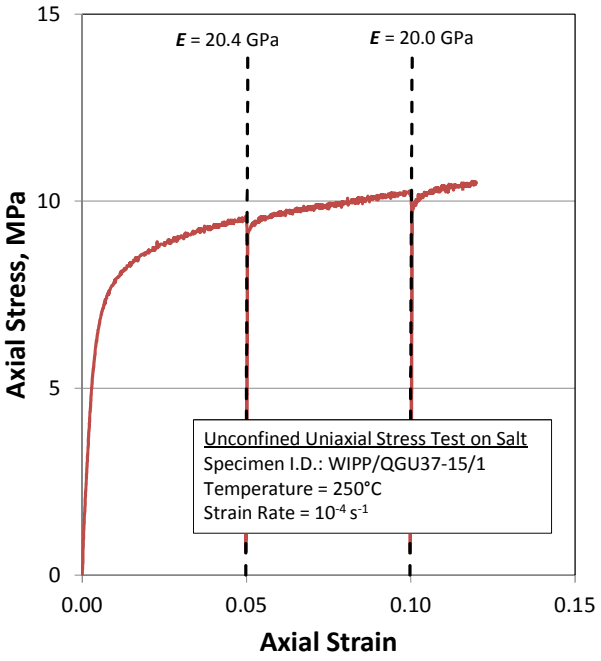

Fig. 10. Unload/reload cycles on specimen WIPP/QGU37-15/1 at 250°C.

The plots in Figure 9 are dominated by the stress-relaxation stage of the test where the axial strain was held constant at 12% overnight after the initial loading. The axial stress decreased substantially and began to stabilize at near 2 MPa, which indicates significantly more recovery than observed at 200°C. Again, the stress relaxation exhibited undulatory cycles similar to the 200°C test, which will be further examined. The unload/reload cycles provided in Figure 10 are typical for salt because they exhibit very linear (elastic) behavior when the stress is less than the previous maximum stress before unloading. Fits to the linear interval of the reload portion were made as described previously. The final loading to determine the ultimate strength, plotted in Figure 11, was performed identically to the procedure used at 200°C, which resulted in an ultimate axial stress of 12.5 MPa.

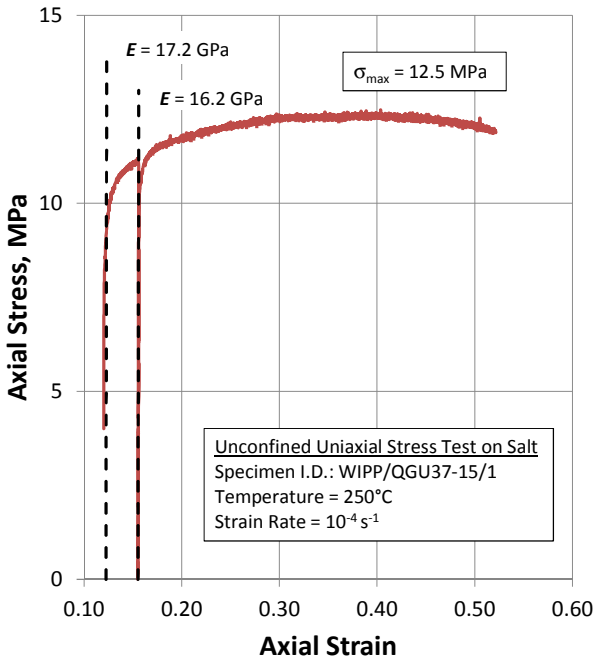

Fig. 11. Final loading to ultimate strength for specimen WIPP/QGU37-15/1 at 250°C.

These unload/reload cycles indicated that the elastic constants had decreased by perhaps as much as 15% or 20% during the stress-relaxation stage. This decrease probably indicates the softening of the salt substructure enhanced by the higher temperature.

Test results are summarized in Table 3. Some general comments are that Young's modulus tends to decrease with an increase in strain or temperature. At higher temperatures, less stress is required to induce specific strain levels, the ultimate strength decreases with an increase in temperature, and the strain at ultimate strength increases with an increase in temperature. In both tests, the specimens sustained extremely high deformations while still maintaining some significant residual strength. Macroscopic vertical cracks became evident near the end of the test when most of the voids were opened. Otherwise, isochoric mechanisms dominated deformation at these temperatures. Figure 12

is a photograph of the two test samples (200°C on the left side and 250°C on the right side). The black arcs on the surface are areas in which thermal conductivity is being measured as a function of damage, but that posttest work is not reported here. The amount of plastic deformation is pronounced; the final damage exhibited in the deformed samples probably accumulated late in the test.

Table 3. Summary of test results

Test I.D. (Temperature)	Strain (%)	Stress (MPa)	*E* (GPa)	Comment
WIPP/ QGU37-20/1 (200°C)	5	11.8	21.3	First unload/reload
	10	13.1	20.7	Second unload/reload
	12	13.4	—	Start of stress relaxation
	12	~4	19.2	End of stress relaxation
	~18	13.6	—	Ultimate strength
	21	12.6	—	Test termination
WIPP/ QGU37-15/1 (250°C)	5	9.6	20.4	First unload/reload
	10	10.2	20.0	Second unload/reload
	12	10.5	—	Start of stress relaxation
	12	~2	17.2	End of stress relaxation
	15.5	11.1	16.2	Unload/reload (LVDT reset)
	~40	12.5	—	Ultimate strength
	52	11.9	—	Test termination

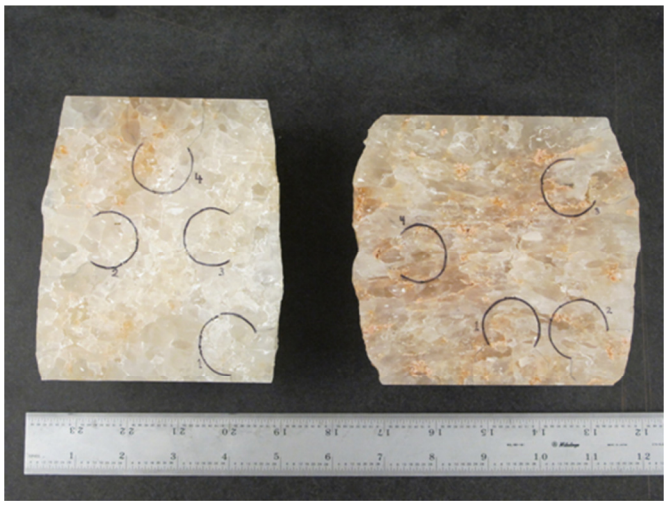

Fig. 12. Uniaxial samples sawn after testing.

4. NUMERICAL ANALYSES

The same load path was used in both successful tests, and that load path can be modeled using finite element software that incorporates a constitutive model for the time-dependent behavior of WIPP salt. For these tests, the specimen response was modeled using the WIPP clean salt parameter values for the Multimechanism Deformation (M-D) creep constitutive model [3] using the thermomechanical finite element program SPECTROM-32 [4]. The WIPP clean salt parameter values were estimated from a body of laboratory test data that was predominantly obtained at temperatures less than 200°C. The numerical analyses were completed before the experiments to assess the ability of the M-D model (parameterized using those lower temperature test results) to predict the behavior of the two uniaxial tests at 200°C and 250°C.

The comparison of the model predictions to the test data for the stress relaxation portion of the load path is shown in Figure 13. The plot also includes the constant strain-rate loading stage that precedes the stress relaxation stage. The constant strain-rate loading at $10^{-4}s^{-1}$ was used to impose an axial strain of 12%. The stress relaxation stage was initiated at this point. As expected, the lower temperature test required more stress to impose the initial strain of 12% than the higher temperature test did. The stress level's quick drop in an exponential fashion during the stress relaxation phase, where the strain level was maintained at 12% for approximately 16 hours, was also expected. The comparison between predictions and test data indicates that the model can reproduce the rate of stress relaxation (creep) very well, but the final predicted stress levels after 16 hours are somewhat lower than the actual test data. The model predictions and test data during the initial loading stage are shown in Figure 14. The sawtooth nature of the predictions is a result of applying incremental displacements. The model does a reasonable job of reproducing the nonlinear behavior of the salt during initial loading, but the predicted stress levels are somewhat higher than those measured in the test.

Both the loading and relaxation results at 250°C were in exceptional agreement (considering these were predictions). This is a positive indication that the model has captured the temperature sensitivities of the micromechanics quite well. The remaining tests will help refine the elevated temperature sensitivity.

5. MICROMECHANICS

Microscopic techniques developed in previous studies, such as the WIPP shaft seal investigations and the observational work completed for the final BAMBUS II report [5], were revitalized and extended for the research reported in this paper. This type of observational work on salt has not been performed in U.S. repository programs for many years, even though the observations made in this paper are based on extensive material developed earlier [6]. Most of the observations made to

date involve etched cleavage chips. Other techniques employed optical microscopy on thick-thin sections and scanning electron microscopy. An optical "thick-thin" section is approximately 5 mm thick. This allows for optical observations on the surface along grain boundaries and through the crystal structure.

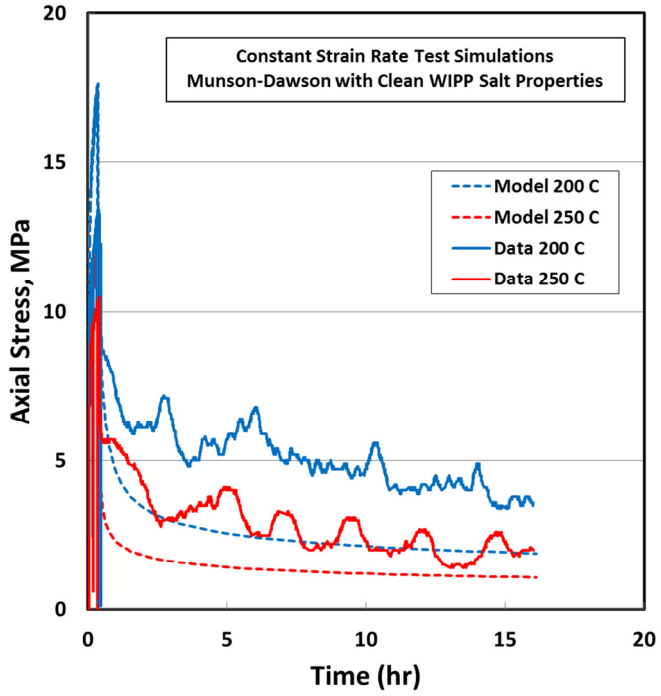

Fig. 13. Comparison of model predictions to test data during stress relaxation stage.

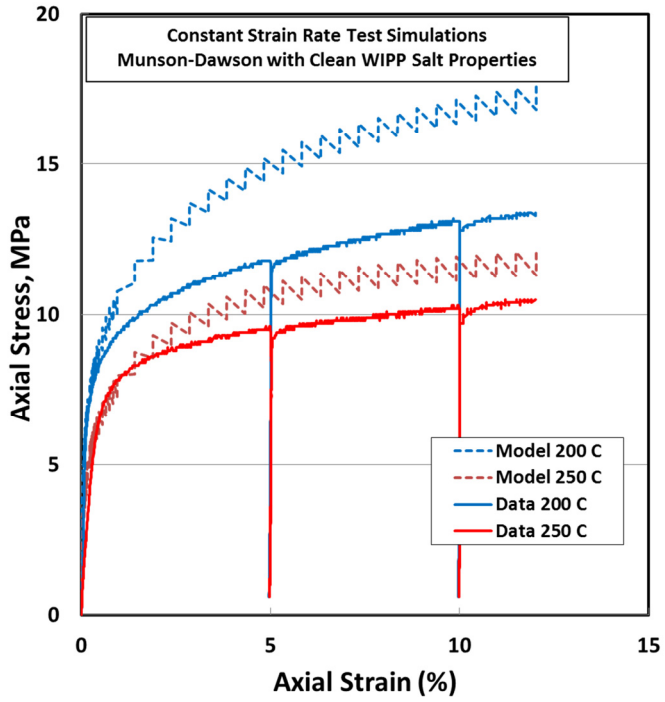

Fig. 14. Comparison of model predictions to test data during initial loading stage.

The plastic deformation of salt is accommodated by progressive mechanisms in order of strain and/or temperature; these are: dislocation multiplication, glide, cross-slip, diffusional processes of climb with glide and core diffusion, and recrystallization. Figure 15 illustrates many of these resulting substructures of deformed salt. The free dislocation density illustrated in the photomicrograph in the upper left was developed at an axial strain of 0.005 and a temperature of 100°C. The field of view is 0.04 mm across the photograph. This substructure is similar to natural Salado Formation salt with a free dislocation density around 2.3 (10^7) cm^{-2} and a subgrain diameter of 340 µm. The center photomicrograph is an example of glide with cross slip developed within a sample deformed to an axial strain of 0.15 at 70°C. The wavy glide bands developed on (110) planes with orthogonal conjugate plane contribution. The field of view is 0.1 mm across the photograph. Salt plasticity promoted by slip or glide along the (110) plane has been well documented in many laboratory tests on intact salt [7]. The example of polygonization was deformed at 200°C at a differential stress of 5 MPa to an axial strain of 0.10. The field of view is 0.1 mm across. The substructures shown in Figure 15 were all developed in confined tests. We will examine the substructures of salt deformed at temperatures beyond 200°C and unconfined conditions to help assess the extension of the existing creep database.

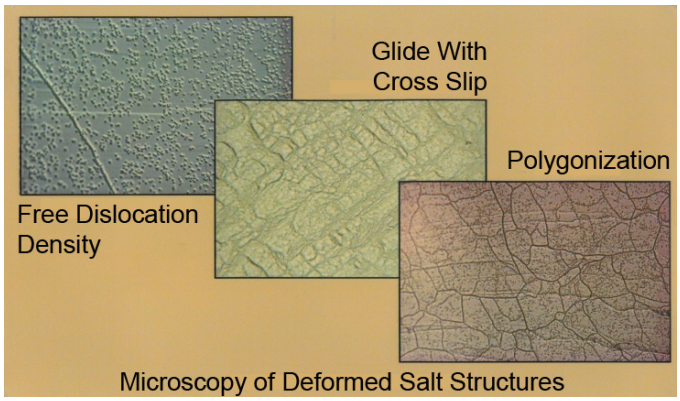

Fig. 15. Evolution of micromechanisms.

The highly distorted grains were cleaved with some difficulty. One can qualitatively appreciate the internal deformation of the cleaved chips by comparing its fabric to similar cleavage chips of native Permian salt. Natural salt typically cleaves nearly perfectly planar and exhibits few cleavage steps along the surface. By contrast, the deformed salt exhibits crenulations on the (100) plane itself in the form of small-scale folding superimposed on the cleavage plane. After deformed grains were extracted, they were etched for 2 to 3 seconds in methanol saturated with $PbCl_2$ and stopped in butanol. Figure 16 captures two photomicrographs of the substructure after deformation at 250°C. The upper photograph (B) exemplifies a completely recovered substructure that is essentially devoid of glide bands and subgrain boundaries; only dispersed free dislocations can

be seen. Well-developed subgrains and low dislocation density are captured in the lower photo (A), which is taken from the same sample. These substructures are both indicative of thermally activated climb recovery and annealing.

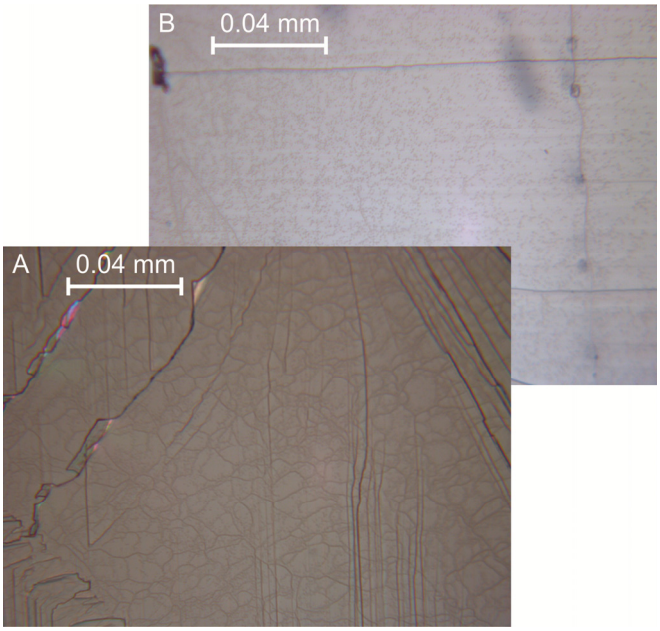

Fig. 16. Etched cleavage chip from 250°C uniaxial test.

Under these conditions, the intact salt would be considered relatively soft because it has few dislocations or glide band tangles. A softer substructure is consistent with the observed lower modulus and lower ultimate strength.

6. CONCLUSIONS

This initial suite of uniaxial tests explored salt behavior under severe temperatures to document its plastic response and, at the same time, evaluate the extrapolation of the M-D creep model to temperatures outside its previous database. The numerical model does a reasonable job of reproducing the nonlinear behavior of the salt but could be improved by an expanded, higher temperature test database for determining the model parameters. The test results clearly demonstrate that the WIPP salt decrepitates violently at temperatures of approximately 280°C when the specimens are unconfined. This behavior probably was not affected by changing heating rates because the decrepitation is attributed to a thermally driven pressure increase in entrapped brine inclusions. Under confined conditions, the pressurized brine inclusions may not cause decrepitation in the same dramatic sense seen here. Predictions of the test results substantiated that the M-D parameterization model reasonably extrapolates outside of its dataset. Also, the unconfined state at these temperatures is sufficiently plastic that deformation processes give rise to behavior similar to an isochoric deformation experienced under confined conditions.

The results obtained in these reconnaissance experiments will be further corroborated with additional testing. This first-of-its-kind information provides insight for the possible disposal of heat-generating waste in salt and any field demonstrations that might be conducted.

REFERENCES

1. Hansen, F.D., S.J. Bauer, S.T. Broome, and G.D. Callahan. 2012. *Coupled thermal-hydrological-mechanical-processes in salt: hot granular salt consolidation, constitutive model and micromechanics*. SAND2012-9893P. DOE FCRD-UFD-2012-000422. Albuquerque, NM: Sandia National Laboratories.

2. Bradshaw, R.L. and W.C. McClain, 1971. *Project salt vault: a demonstration of the disposal of high activity solidified wastes in underground salt mines.* ORNL-4555. prepared by Oak Ridge National Laboratory for the U.S. Atomic Energy Commission.

3. Munson, D.E., A.F. Fossum, and P.E. Senseny, 1989. *Advances in resolution of discrepancies between predicted and measured in situ WIPP room closures.* SAND88-2948, Albuquerque, NM: Sandia National Laboratories.

4. Callahan, G.D., A.F. Fossum, and D.K. Svalstad, 1989. *Documentation of SPECTROM-32: a finite element thermomechanical stress analysis program*. Vol. I and II. DOE/CH/10378-2. prepared by RE/SPEC Inc., Rapid City, SD, for the U.S. Department of Energy, Chicago Operations Office, Argonne, IL.

5. Bechthold, W., E. Smailos, S. Heusermann, T. Bollingerfehr, B. Bazargan Sabet, T. Rothfuchs, P. Kamlot, J. Grupa, S. Olivella, and F.D. Hansen. 2004. *Backfilling and sealing of underground repositories for radioactive waste in salt*. BAMBUS II Project: final report. Call No: EUR 20621 EN. European Commission. Directorate General for Research. Office for Official Publications of the European Communities.

6. Carter, N.L., F.D. Hansen, and P.E. Senseny. 1982. Stress magnitudes in natural rock salt. *J. Geophys. Res.* 87: 9289-9300.

7. Hansen, F.D. 1985. *Deformation mechanisms of experimentally deformed Salina Basin bedded salt.* BMI/ONWI-552. Battelle Memorial Institute. Columbus, OH: Office of Nuclear Waste Isolation.